

# Stationary and Nonstationary Ion and Water Flux Interactions in Kidney Proximal Tubule: Mathematical Analysis of Isosmotic Transport by a Minimalistic Model



Erik Hviid Larsen and Jens Nørkær Sørensen

## Contents

1	Introduction .....	102
2	Description of the Minimalistic Model .....	104
2.1	Functional Organization of Proximal Tubule Epithelium .....	104
2.2	Solute Flux Equations .....	105
2.3	Water Flux Equations .....	111
2.4	Compliant Model and Volumes of Intraepithelial Compartments .....	113
2.5	Electrical-Circuit Analysis .....	113
2.6	Nomenclature and Sign Conventions .....	114
2.7	Numerical Methods .....	115
2.8	Choice of Independent Variables .....	116
2.9	Geometrical Dimensions and Units of Physical Quantities .....	117
3	Results .....	117
3.1	General Features .....	117
3.2	A Component of Na <sup>+</sup> Uptake Bypasses the Pump .....	119
3.3	Inhibition of the Na <sup>+</sup> /K <sup>+</sup> Pump .....	121
3.4	Effect of Adding Glucose .....	122
3.5	Blocking Water Channels of Apical Membrane .....	125
3.6	Volume Response of the Epithelium to a Luminal Osmotic Pulse .....	129
3.7	Uphill Water Transport and Intraepithelial Water Fluxes .....	130
3.8	Isosmotic Transport .....	132
4	Discussion .....	135
4.1	The Coupling Between Active Sodium Transport and Fluid Uptake .....	135
4.2	Eliminating the Osmotic Permeability of Apical Membrane .....	136

---

The original version of this chapter was revised. A correction to this chapter can be found at [https://doi.org/10.1007/112\\_2020\\_40](https://doi.org/10.1007/112_2020_40)

E. H. Larsen (✉)  
Department of Biology, University of Copenhagen, Copenhagen, Denmark  
e-mail: [ehlarsen@bio.ku.dk](mailto:ehlarsen@bio.ku.dk)

J. N. Sørensen  
Department of Wind Energy, Technical University of Denmark, Lyngby, Denmark  
e-mail: [jnso@dtu.dk](mailto:jnso@dtu.dk)

4.3	Transepithelial Osmotic Permeability Versus Osmotic Permeability of Individual Membranes .....	137
4.4	Truly Isosmotic Transport .....	138
5	Additional Information .....	139
	Appendix 1: Nomenclature .....	139
	Appendix 2: Independent Variables .....	140
	References .....	142

**Abstract** Our mathematical model of epithelial transport (Larsen et al. *Acta Physiol.* 195:171–186, 2009) is extended by equations for currents and conductance of apical SGLT2. With independent variables of the physiological parameter space, the model reproduces intracellular solute concentrations, ion and water fluxes, and electrophysiology of proximal convoluted tubule. The following were shown:

1. Water flux is given by active  $\text{Na}^+$  flux into lateral spaces, while osmolarity of absorbed fluid depends on osmotic permeability of apical membranes.
2. Following aquaporin “knock-out,” water uptake is not reduced but redirected to the paracellular pathway.
3. Reported decrease in epithelial water uptake in aquaporin-1 knock-out mouse is caused by downregulation of active  $\text{Na}^+$  absorption.
4. Luminal glucose stimulates  $\text{Na}^+$  uptake by instantaneous depolarization-induced pump activity (“cross-talk”) and delayed stimulation because of slow rise in intracellular  $[\text{Na}^+]$ .
5. Rate of fluid absorption and flux of active  $\text{K}^+$  absorption would have to be attuned at epithelial cell level for the  $[\text{K}^+]$  of the absorbate being in the physiological range of interstitial  $[\text{K}^+]$ .
6. Following unilateral osmotic perturbation, time course of water fluxes between intraepithelial compartments provides physical explanation for the transepithelial osmotic permeability being orders of magnitude smaller than cell membranes’ osmotic permeability.
7. Fluid absorption is always hyperosmotic to bath.
8. Deviation from isosmotic absorption is increased in presence of glucose contrasting experimental studies showing isosmotic transport being independent of glucose uptake.
9. For achieving isosmotic transport, the cost of  $\text{Na}^+$  recirculation is predicted to be but a few percent of the energy consumption of  $\text{Na}^+/\text{K}^+$  pumps.

**Keywords** AQP-1 knock-out · Glucose absorption · Isosmotic transport · Kidney proximal tubule · Mathematical-modeling · Osmotic permeability · Time dependent- and stationary states of water and ion fluxes

## 1 Introduction

In the study from A. K. Solomon’s laboratory of *Necturus* proximal tubule in which net flux of  $\text{NaCl}$  and water were measured over the same period of time, reabsorbed fluid was isosmotic over a wide range of water fluxes. In the phrasing of the authors (Windhager et al. 1959), “water transport in the proximal tubule depends on the

tubular NaCl concentration rather than upon the water activity,” and “the driving force for water movement arises from the efflux of NaCl from tubule to plasma,” which was shown to be inhibited by the  $\text{Na}^+/\text{K}^+$ -ATPase inhibitor ouabain (Schatzmann et al. 1958). Work from several groups confirmed isosmotic transport by kidney proximal tubule (Bennett et al. 1967; Kokko et al. 1971; Morel and Murayama 1970; Schafer et al. 1974) and by other low-resistance epithelia (Curran 1960; Diamond 1964). More recently, isosmotic transport was also observed in high-resistance epithelia (Gaeggeler et al. 2011; Nielsen and Larsen 2007; Schafer 1993), indicating that the ability to transport water at osmotic equilibrium energized by the  $\text{Na}^+/\text{K}^+$ -ATPase is a general feature of transporting epithelia. This may occur even against an adverse osmotic gradient, confirming that epithelia are capable of spending metabolic energy to move water (Diamond 1964; Green et al. 1991; Nielsen and Larsen 2007; Parsons and Wingate 1958). The mechanism of isosmotic transport is debated (Andreoli and Schafer 1979; Fischbarg 2010; Larsen et al. 2009; Nedergaard et al. 1999; Spring 1999; Tripathi and Boulpaep 1989; Whittombury and Reuss 1992; Zeuthen 2000; Zeuthen et al. 2001). Since  $\text{Na}^+/\text{K}^+$  pumps are expressed in membranes lining the lateral intercellular space (DiBona and Mills 1979; Maunsbach and Boulpaep 1991; Mills et al. 1977; Padilla-Benavides et al. 2010; Stirling 1972) similarly to aquaporin water channels (Agre et al. 1993b), it is generally accepted that this space by way of osmosis couples the active  $\text{Na}^+$  flux and the water flux and that isosmotic transport simply follows from a large water permeability (Altenberg and Reuss 2013).

Weinstein and Stephenson (1981) established tradition for applying mathematical formalisms in the analysis of steady state water and ion absorption by kidney proximal tubule (Weinstein 1986, 1992, 2013). Our steady state mathematical models of leaky epithelia (Larsen et al. 2000, 2002) have been expanded for computing time-dependent states (Larsen et al. 2009). The present analytical model comprising new apical glucose transport equations and comprehensive mathematical handling of electrical properties enables us to confront quantitatively computations with crucial experiments on kidney proximal tubule.

The present study has a dual purpose. Firstly, we present in detail complex relationships between active ion fluxes and water flows in an epithelium of extremely large membrane hydraulic permeabilities, as exemplified by mammalian proximal tubule of amplified apical and lateral plasma membrane areas (Welling and Welling 1975, 1988), which make this nephron segment one of the most water-permeable epithelia in nature (Carpi-Medina et al. 1983; Schafer 1990). This is done by quantitative analysis of a mathematical model which comprises cellular and paracellular pathways for fluxes of ions, glucose, and water. It is an important quality of our treatment that water absorption is governed by a driving force resulting from solute fluxes and intraepithelial solute solvent coupling reflecting the conditions in vivo (Gottschalk 1963) and in microperfused isolated tubules (Green et al. 1991). By including glucose and electrical properties, commonly applied laboratory protocols can be simulated for investigating the explanatory power of the model over a wide range of observations. Besides analysis of relationships between volume flows and solute fluxes, our analysis comprises time-dependent states evoked by

perturbation of, e.g., osmolarity of external solutions or “knock-out” of a specific membrane transporter providing novel insight into redistributions of water flows between cells and paracellular space.

The second purpose of the study is to analyse in the depth problems of importance for the function of vertebrate kidney that hitherto have been out of focus. Examples are the conflict between osmotic permeability of whole epithelium and that of individual membranes, with reference to the studies from Solomon’s laboratory discussed above; the relative significance of sodium pump activity to aquaporin water channel osmotic permeability for the rate of water absorption; robustness of mathematical solutions giving isosmotic absorption; and the relative significance of transcellular and paracellular fluid absorption, respectively. Our analysis of every one of these problems provides novel information of definitive and general nature.

## 2 Description of the Minimalistic Model

### 2.1 *Functional Organization of Proximal Tubule Epithelium*

Mammalian proximal tubule is a heterocellular epithelium with three consecutive segments of individual functional and structural complexity (Maunsbach 1966; Welling and Welling 1988; Zhuo and Li 2013). All segments are engaged in isosmotic fluid absorption energized by lateral  $\text{Na}^+/\text{K}^+$  pumps. The minimalistic model epithelium reproduces  $\text{Na}^+$ -coupled water transport in all three segments, and by having lumen-negative transepithelial potential difference and water absorption coupled predominantly to absorption of  $\text{NaCl}$  and glucose, the model epithelium has these features in common with the proximal convoluted tubule. It follows that the model discussed here does not handle acid-base transport and cannot, therefore, reproduce absorption of bicarbonate ions. However, by containing the essential module of subcellular complexity driving isosmotic transport, all conclusions of the present study apply to all three segments – and generally to other transporting epithelia.

The width of the lateral space (distance between neighbouring cells) is constant while neighbouring cells interdigitate in progressively more complicated way toward the cell base (Maunsbach 1973; Welling and Welling 1988). A quantitative stereologic study of size and shape of cells and lateral intercellular spaces (*lis*) of all three segments of proximal tubule indicated similar relatively large areas of apical membrane (comprising brush border surface and intervening membrane) and lateral membrane (Welling and Welling 1988). The area of serosal membrane contacting the basement membrane is much smaller than those of the above two membrane domains. The interspace basement membrane providing exit from the lateral intercellular space is about 10% of the area of the entire basement membrane. Morphometric analyses further indicated that the so-called basal infoldings do not stem from serosal membrane contacting the basement membrane but represent a

complex lateral-membrane arrangement of arbitrary orientation in the basal 20% region of tubule cells (Welling et al. 1987a). A fluorometric micro-assay of  $\text{Na}^+/\text{K}^+$ -ATPase (Garg et al. 1981) demonstrated highest expression of this enzyme in proximal convoluted tubule as compared to downstream segments of the nephron, and net  $\text{Na}^+$  transport previously measured in microperfused tubule segments correlated well with their  $\text{Na}^+/\text{K}^+$ -ATPase activity. Immunocytochemical studies localized the  $\text{Na}^+/\text{K}^+$ -ATPase to lateral plasma membranes and to the abovementioned complex of lateral plasma membrane infoldings at the base of tubule cells (Kashgarian et al. 1985; Maunsbach and Boulpaep 1991). Immunocytochemical reaction was not observed on those areas of the basal plasma membrane directly contacting basal lamina (Kashgarian et al. 1985) nor is this transporter found on the luminal brush border (Jørgensen 1986). This agrees with studies on localization of [ $^3\text{H}$ ]-ouabain in other transporting epithelia (DiBona and Mills 1979; Mills and DiBona 1977, 1978; Stirling 1972). In ileal intestinal mucosa, a thyroid epithelial FRT-cell line, and MDCK cells grown as a confluent monolayer on permeable filter support is the  $\text{Na}^+/\text{K}^+$ -ATPase present in lateral membranes of cells with no immunofluorescent staining neither at apical nor at serosal cell surfaces (Amerongen et al. 1989; Padilla-Benavides et al. 2010; Zurzolo and Rodriguezboulouan 1993). Thus, in transporting epithelia, the lateral plasma membrane and the serosal plasma membrane constitute different functional domains implying that sodium ions transported into the cell through the apical plasma membrane are actively transported into *l<sub>is</sub>* for exiting the epithelium through the interspace basement membrane. Because the so-called “basolateral” osmotic permeability identified as AQP-1 (Agre et al. 1993a, b) is confined to the lateral membrane, the lateral intercellular space constitutes a compartment of its own with physically well-defined boundary toward the serosal (interstitial) compartment as depicted in Fig. 1a. Thus, for transepithelial osmotic equilibrium, water entering the epithelium through any membrane domain leaves the epithelium through the interspace basement membrane. This applies even if the serosal cell membrane’s osmotic permeability is non-zero and follows from a slightly hyperosmotic cell water driving water into the cell not only from luminal solution but also from serosal bath. The above functional organization constitutes the prerequisite for truly isosmotic transport. Thus, quantitative analysis of water uptake by our minimalistic model provides insight into isosmotic transport by absorbing epithelia in general.

## 2.2 Solute Flux Equations

The computations presented in this paper do not depend on any particular assumption about the nature of luminal entrance mechanisms as long as we keep absolute ion fluxes and water flows in agreement with measured quantities. With this requirement being fulfilled, there are additional features of the minimalistic model

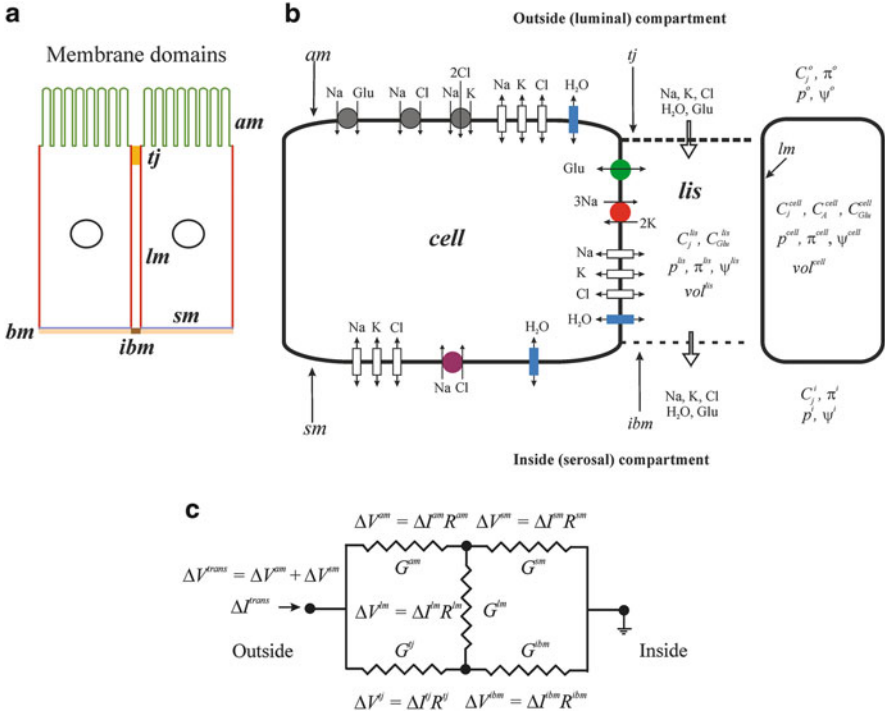


**Fig. 1** (a) Cell membranes of transporting epithelia constitute three functionally different domains. Localization of fluorescence probes or radioactive  $^3\text{H}$ -labeling of antibodies raised against transport proteins indicated that lateral and serosal membranes constitute functionally different domains; see text for references. As a consequence, the notion “basolateral membrane” would have to be avoided. *am* apical membrane with microvilli, *tj* tight junction, *lm* lateral membrane, *sm* serosal membrane, *bm* basement membrane in light brown color that includes the interspace basement membrane, *ibm* indicated by darker brown color. (b) Transport systems of the minimalistic epithelial model with definitions and nomenclature. Transport systems and symbols as defined in text and Appendix 1 and 2. In the investigation of conditions for obtaining truly isosmotic transport is the 1  $\text{Na}^+$ : 1  $\text{Cl}^-$  cotransporter activated for obtaining an overall isosmotic transport (see text for further explanation). (c) The five membranes of the epithelium constitute a bridge circuit. The solution to the mathematical problem for a given set of independent variables contains values of the five membrane resistors indicated above. The resistance of the bridge circuit, however, cannot be calculated according to rules for series and parallel resistors. Therefore, it is computed by simulating a current injection,  $\Delta I^{\text{trans}}$ , and applying Kirchhoff’s rules for solving the set of five current equations by the “solve routine” of *Mathematica*©. Subsequently, the five membrane currents,  $\Delta I^m$ , are used for calculating change in membrane potentials, transepithelial resistance ( $R^{\text{trans}} = \Delta V^{\text{trans}} / \Delta I^{\text{trans}}$ ), and fractional resistance of the apical membrane. The resistance notation in *Mathematica*© equations are defined as follows:  $R^{\text{am}} = R_1$ ,  $R^{\text{sm}} = R_2$ ,  $R^{\text{lm}} = R_3$ ,  $R^{\text{tj}} = R_4$ , and  $R^{\text{ibm}} = R_5$ . See methods for details

that would have to be met for our purpose. In the absence of glucose and amino acids, Frömter’s seminal study reported a fairly large apical membrane conductance of about  $4 \text{ mS cm}^{-2}$  with a ratio of the resistance of the luminal membrane to the transepithelial resistance of 0.8 (Frömter 1982). In the cell, both  $\text{K}^+$  and  $\text{Cl}^-$  are above

thermodynamic equilibrium (Cassola et al. 1983; Edelman et al. 1978; Windhager 1979). Since neither is secreted into the luminal solution, the above electrical conductance is governed predominantly by a Na<sup>+</sup> conductance. A Na<sup>+</sup> conductance is associated with the 3 Na<sup>+</sup>:1HPO<sub>4</sub><sup>2-</sup> cotransporter. Frömter (1982) perfused the kidney tubule with physiological saline containing 1 mM HPO<sub>4</sub><sup>2-</sup>; thus with a coupling ratio of 3 Na<sup>+</sup>:1HPO<sub>4</sub><sup>2-</sup>, it is unlikely that this transporter accounts for the relatively very large conductance of 4 mS/cm<sup>2</sup>, which leaves a Na<sup>+</sup> channel as the most likely candidate for the Na<sup>+</sup> conductance of the apical membrane. This goes along with the study by Morel and Murayama (1970), who obtained isosmotic reabsorption in microperfused rat proximal tubule in the absence of phosphate ions in the luminal perfusion solution. Added to this, a sodium ion channel was disclosed by patch clamp of rabbit proximal straight tubule (Gögelein and Greger 1986). The Goldman-Hodgkin-Katz (GHK) constant field equations are applied for handling this as well as electrodiffusion fluxes in the other ion channels including tight junction and interspace basement membrane (Goldman 1943; Hodgkin and Katz 1949; Sten-Knudsen 2002):

$$J_j = \left( \frac{z_j F V}{RT} P_j \right) \frac{C_j^{(I)} \exp[z_j F V / (RT)] - C_j^{(II)}}{\exp[z_j F V / (RT)] - 1} \quad (1a)$$

The associated chord conductance is:

$$G_j = \left( \frac{(z_j F)^2 V}{RT} P_j \right) \frac{C_j^{(I)} \exp[z_j F V / (RT)] - C_j^{(II)}}{(\exp[z_j F V / (RT)] - 1) (V - V_j^{eq})} \quad (1b)$$

$P_j$  is the ion permeability and  $V$  potential difference across the membrane. I = *lumen* and II = *cell* for the apical membrane, I = *cell* and II = *lis* for the lateral membrane, and I = *cell* and II = *serosa* for the serosal membrane. The proximal tubule reabsorbs 50–70% of the filtered K<sup>+</sup> load. Wilson et al. (1997) showed that cyanide caused a reduction in net potassium flux over the entire range of fluid fluxes in their double-perfusion experiments. Subsequent single-perfusion experiments (tubule lumen only) using the specific K<sup>+</sup>-H<sup>+</sup>-ATPase inhibitor, SCH28080, did not reveal evidence for primary active K<sup>+</sup> absorption. The authors discussed the possibility that tubular absorption of K<sup>+</sup> is accomplished by paracellular solvent drag. This mechanism is included in our model and will be quantitatively evaluated in Results for concluding that solvent drag cannot account for transtubular absorption of K<sup>+</sup>. The principal importance of active K<sup>+</sup> absorption is independent of the molecular design of the transporter. It is of importance, however, that the transepithelial active flux of potassium ions results in a K<sup>+</sup> concentration of the absorbate that is close to the concentration of K<sup>+</sup> in serosal fluid. The K<sup>+</sup> absorption against the prevailing small transepithelial electrochemical potential difference shall be accounted for by assuming (1Na<sup>+</sup>, 1K<sup>+</sup>, 2Cl<sup>-</sup>) cotransport across the apical membrane:

$$J_j^{NaK2Cl,m} = r \cdot K^{NaK2Cl,m} \left[ C_{Na}^{(I)} \cdot C_K^{(I)} \cdot \left( C_{Cl}^{(I)} \right)^2 - C_{Na}^{(II)} \cdot C_K^{(II)} \cdot \left( C_{Cl}^{(II)} \right)^2 \right] \quad (2a)$$

Here,  $r = 1$  for  $Na^+$  and  $K^+$  and  $r = 2$  for  $Cl^-$ . In agreement with cellular  $Cl^-$  accumulation via a  $Na^+$ -dependent cotransporter in *Necturus* (Spring and Kimura 1978, 1979) and rat (Karniski and Aronson 1987; Warnock and Lucci 1979), we assume that a  $(1Na^+, 1Cl^-)$  cotransporter is present in the apical membrane:

$$J_j^{NaCl,m} = K^{NaCl,m} \left[ C_{Na}^{(I)} \cdot \left( C_{Cl}^{(I)} \right) - C_{Na}^{(II)} \cdot \left( C_{Cl}^{(II)} \right) \right] \quad (2b)$$

For generalizing the description, apical  $Cl^-$  and  $K^+$  channels are included, but in the present calculations, they do not carry significant fluxes because they are largely quiescent under normal conditions (Boron and Boulpaep 2017).

In 1976, a sodium ion/proton antiporter was discovered in vesicles isolated from renal brush-border membranes of rat by Murer et al. (1976); it was cloned and named NHE3 (Sardet et al. 1989). As recently reviewed by Zhuo and Li (2013), subsequent studies confirmed its function as pathway for eliminating protons in exchange for luminal sodium ions in kidney proximal nephron. The NHE3 antiporter operates in series with a lateral electrogenic cotransporter of stoichiometry  $1 Na^+:3 HCO_3^-$ . Bicarbonate is regenerated from  $OH^-$  and  $CO_2$  catalyzed by a cytoplasmic carbonic anhydrase (Boron and Boulpaep 2017). The operation of this enzyme together with the NHE3 antiporter is assumed to recover quantitatively  $HCO_3^-$ , which is transported together with sodium ions into the interstitial fluid (Boron and Boulpaep 1983a, b; Yoshitomi et al. 1985). At this stage of our studies, we aim at transport features that are independent of acid-base transporters. As shall be demonstrated below, this “minimalistic” model is excellently suited for analysis of general features of isosmotic transport, e.g., none of our conclusions are being affected by this simplification.

Driving forces for glucose uptake across the luminal membrane of rat convoluted proximal tubule are the transmembrane  $Na^+$  concentration gradient, the transmembrane glucose concentration gradient, and the membrane potential. The transporter saturates with luminal  $Na^+$  concentration as well as with luminal glucose concentration (Samarzija et al. 1982). Glucose is coupled to  $Na^+$  uptake by the  $Na^+/D$ -glucose cotransporter-2 (SGLT2) with a stoichiometry of  $1 Na^+:1$  glucose in tubule segments S1 and S2 and  $Na^+/D$ -glucose cotransporter-1 (SGLT1) with a stoichiometry of  $2 Na^+:1$  glucose in tubule segments S3 (Ghezzi et al. 2018; Hummel et al. 2011; Parent et al. 1992; Turner and Moran 1982; Turner and Silverman 1977). SGLT2 is rheogenic, and with 150 mM external  $Na^+$  concentration, the transporter generates a nonlinear current-voltage relationship reflecting voltage dependence of the  $Na^+$  current (Hummel et al. 2011; Parent et al. 1992). With sign conventions in epithelial studies, inward  $Na^+$  currents are positive and  $V^{am} = \psi^o - \psi^{cell}$  with the associated current-voltage relationship being upward concave. This corresponds to the downward concave current-voltage relationship obtained with SGLT2 expressed in *Xenopus* oocyte (Parent et al. 1992) or HEK293T cells (Hummel et al. 2011) where inward  $Na^+$  currents are given a negative sign, and membrane potential is defined as  $V = \psi^{cell} - \psi^o$ . The last mentioned studies reported zero



SGLT2-current in the absence of external glucose or in the absence of external  $\text{Na}^+$ . Thus, in the absence of luminal glucose, the  $\text{Na}^+$  conductance of SGLT2 is zero. Finally, the reversal potential of the SGLT2-cotransporter  $E_{rev}^{am, Glu-Na}$  would have to fulfill the requirement that Gibbs free energy remains constant following one transport cycle as expressed by (Schultz 1980):

$$E_{rev}^{am, Glu-Na} = \frac{RT}{F} \ln \frac{C_{Glu}^o \cdot C_{Na}^o}{C_{Glu}^{cell} \cdot C_{Na}^{cell}}$$

The abovementioned requirements are fulfilled by the following set of equations:

$$J_{Na}^{am, Glu-Na} = \left( \frac{P^{Glu-Na} F V^{am}}{RT} \right) \left( \frac{C_{Glu}^o}{K_{Glu}^{Glu-Na} + C_{Glu}^o} \right) \left( \frac{C_{Na}^o}{K_{Na}^{Glu-Na} + C_{Na}^o} \right) \\ \times \frac{C_{Glu}^o C_{Na}^o \exp\{FV^{am}/(RT)\} - C_{Glu}^{cell} C_{Na}^{cell}}{\exp\{FV^{am}/(RT)\} - 1} \\ J_{Glu}^{am, Glu-Na} = J_{Na}^{am, Glu-Na} \\ V^{am} = \psi^o - \psi^{cell} \quad (3a)$$

$P^{Glu-Na^+}$  is the maximal turnover of SGLT2, where  $K_{Glu}^{Glu-Na^+} \approx 5$  mM and  $K_{Na^+}^{Glu-Na^+} \approx 25$  mM are apparent dissociation constants of the transporter's binding sites (Hummel et al. 2011). For obtaining the associated chord (integral) conductance, the current carried by SGLT2 is introduced and multiplied by unity expressed as  $(V^{am} - E_{rev}^{am, Glu}) / (V^{am} - E_{rev}^{am, Glu})$ :

$$I_{Na}^{am, Glu-Na} = \frac{P' F^2 V^{am} [C_{Glu}^o C_{Na}^o \exp\{FV^{am}/(RT)\} - C_{Glu}^{cell} C_{Na}^{cell}]}{RT[\exp\{FV^{am}/(RT)\} - 1](V^{am} - E_{rev}^{am, Glu})} (V^{am} - E_{rev}^{am, Glu}) \quad (3b)$$

By having the form  $I_j = G_j (V_m - E_j)$ , the integral conductance is calculated from:

$$G_{Na}^{am, Glu-Na} = \frac{P' F^2 V^{am} [C_{Glu}^o C_{Na}^o - C_{Glu}^{cell} C_{Na}^{cell} \exp\{FV^{am}/(RT)\}]}{RT[\exp\{FV^{am}/(RT)\} - 1](V^{am} - E_{rev}^{am, Glu})} \quad (3c)$$

where  $E_{rev}^{am, Glu-Na}$  is given by Eq. (3b) and  $P'$  by:

$$P' = P^{Glu-Na} \left( \frac{C_{Glu}^o}{K_{Glu}^{Glu-Na} + C_{Glu}^o} \right) \left( \frac{C_{Na}^o}{K_{Na^+}^{Glu-Na} + C_{Na}^o} \right) \quad (3d)$$

Other SGLT2-models also handle saturation kinetics and substrate interactions, e.g., Layton et al. (2015) and Weinstein (1985). Unlike these previous treatments, Eqs. (3a–3d) cover the transporter's contributions to membrane potential and

membrane conductance; in the present study, this is required for its validation by comparing computations with experiments.

Immuno-labeling has shown that  $\text{Na}^+/\text{K}^+$ -ATPase (Skou 1965) is expressed exclusively in lateral plasma membrane (Kashgarian et al. 1985). The active cation fluxes are saturating function of cell  $\text{Na}^+$  ( $C_{\text{Na}}^{\text{cell}}$ ) and concentration of  $\text{K}^+$  in lateral intercellular space ( $C_{\text{K}}^{\text{lis}}$ ) (Garay and Garrahan 1973; Goldin 1977; Jørgensen 1980). The pump rate is also a function of the electrical work done in moving one charge across the membrane per pump cycle (Thomas 1972), which is a function of lateral membrane potential,  $V^{\text{lm}}$ , and the electrical work contributed by the pump-ATPase, here denoted  $E^{\text{pump}}$ . The above properties are fulfilled by the following set of equations (Larsen et al. 2009):

$$\begin{aligned} j_{\text{Na}}^{\text{lm,pump}} &= \frac{P_{\text{Na,K}}^{\text{lm,pump}}}{F} \left( \frac{C_{\text{Na}}^{\text{cell}}}{K_{\text{Na}}^{\text{lm,pump}} + C_{\text{Na}}^{\text{cell}}} \right)^3 \left( \frac{C_{\text{K}}^{\text{lis}}}{K_{\text{K}}^{\text{lm,pump}} + C_{\text{K}}^{\text{lis}}} \right)^2 [V^{\text{lm}} + E^{\text{pump}}] \\ j_{\text{K}}^{\text{lm,pump}} &= -\frac{2}{3} j_{\text{Na}}^{\text{lm,pump}} \\ V^{\text{lm}} &= \psi^{\text{cell}} - \psi^{\text{lis}} \end{aligned} \quad (4a)$$

$\frac{P_{\text{Na,K}}^{\text{lm,pump}}}{F}$  of dimension of  $\text{mol s}^{-1} \text{V}^{-1}$  per unit area of plasma membrane represents the  $\text{Na}^+$  efflux through the sodium pump saturated with internal  $\text{Na}^+$  and external  $\text{K}^+$  at normal cytoplasmic ATP levels. With a 3  $\text{Na}^+$ :2  $\text{K}^+$  stoichiometry, the expression for the pump current is:

$$I^{\text{lm,pump}} = \frac{P_{\text{Na,K}}^{\text{lm,pump}}}{3} \left( \frac{C_{\text{Na}}^{\text{cell}}}{K_{\text{Na}}^{\text{lm,pump}} + C_{\text{Na}}^{\text{cell}}} \right)^3 \left( \frac{C_{\text{K}}^{\text{lis}}}{K_{\text{K}}^{\text{lm,pump}} + C_{\text{K}}^{\text{lis}}} \right)^2 [V^{\text{lm}} + E^{\text{pump}}] \quad (4b)$$

Eq. (4b) gives pump currents that are linearly dependent on membrane potential, which is an acceptable approximation for the interval,  $-110 \text{ mV} < V^{\text{lm}} < -5 \text{ mV}$  (Gadsby and Nakao 1989; Lauger 1991; Wu and Civan 1991) that covers computations of the present study. The reversal potential of pump currents is  $E_{\text{rev}}^{\text{pump}} = -E^{\text{pump}}$  with free energy of ATP hydrolysis,  $\Delta G_{\text{ATP}} \approx -60 \text{ kJ/mol}$  and stoichiometry of 3  $\text{Na}^+$ :2  $\text{K}^+$ :1 ATP,  $E^{\text{pump}}$  is about 200 mV which is within the range discussed by de Weer et al. (1988) and used in all our computations independently of the rate of pump flux. Unlike the reversal potential of the  $\text{Na}^+$  pump of a tight epithelium, e.g., frog skin (Larsen 1973; Eskesen and Ussing 1985), the last mentioned assumption is plausible for proximal tubule cells of high density of mitochondria in remarkably close contact with pump sites that would minimize the diffusion distance between sites of dephosphorylation of ATP and rephosphorylation of ADP, respectively (Dørup and Maunsbach 1997). Following Lauger (1991), by inspection of Eq. (4b) in the range indicated where  $P_{\text{Na,K}}^{\text{lm,pump}}$  is considered constant, the integral conductance of the pump would be:

$$G^{lm,pump} = \frac{P_{Na,K}^{lm,pump}}{3} \left( \frac{C_{Na}^{cell}}{K_{Na}^{lm,pump} + C_{Na}^{cell}} \right)^3 \left( \frac{C_K^{lis}}{K_K^{lm,pump} + C_K^{lis}} \right)^2 \quad (4c)$$

Early mathematical models of proximal tubule by Sackin and Boulpaep (1975) and Weinstein (1986, 1992) did not include membrane potential as driving force for pump currents. Other studies included the membrane conductance-dependent electrogenic contribution of the pump to membrane potential (Lew et al. 1979 and Larsen 1991). The above Eq. (4a) is an expansion of previous treatments by acknowledging that potential *per se* is driving force for pump currents. The advantage of this new treatment shall be underscored in Results.

The expression for convection-diffusion of glucose across tight junction and interspace basement membrane obeys the Smoluchowski equation (Smoluchowski 1915). It was derived by Hertz (1922), and when applied to a membrane of reflection coefficient indicated by  $\sigma$ , the expression reads (Larsen et al. 2000):

$$J_{Glu} = J_V(1 - \sigma_{Glu}) \frac{C_{Glu}^{(I)} \exp[J_V(1 - \sigma_{Glu})/P_{Glu}] - C_{Glu}^{(II)}}{\exp[J_V(1 - \sigma_{Glu})/P_{Glu}] - 1} \quad (5)$$

The equation was expanded for covering the convection-electrodifffusion regime (Larsen et al. 2002),

$$J_j = \left( \frac{z_j F V}{RT} P_j + J_V(1 - \sigma_j) \right) \frac{C_j^{(I)} \exp[z_j F V / (RT)] \exp[J_V(1 - \sigma_j)/P_j] - C_j^{(II)}}{\exp[z_j F V / (RT)] \exp[J_V(1 - \sigma_j)/P_j] - 1} \quad (6)$$

Here, it is assumed that the pore is symmetrical such that reflection coefficient and partition coefficient ( $\beta$ ) are related by  $\sigma = (1 - \beta)$  as shown by Finkelstein (1987).  $J_V$  is the volume flux from compartment I (lumen or *lis*) to II (*lis* or *serosa*), and  $\sigma_j$  is the reflection coefficient of ion  $j$  of the membrane. Exit of glucose across lateral membrane is governed by saturation kinetics of a symmetrical carrier (Stein 1967),

$$J_{Glu}^{lm} = J_{Glu}^{lm,max} \frac{K_{Glu}^{lm} (C_{Glu}^c - C_{Glu}^{lis})}{(K_{Glu}^{lm} + C_{Glu}^c) (K_{Glu}^{lm} + C_{Glu}^{lis})} \quad (7)$$

### 2.3 Water Flux Equations

In agreement with cloned aquaporins of proximal tubule (Borgnia et al. 1999), we assume reflection coefficient of unity for water flow through all plasma membranes. Thus, equations for the respective volume fluxes per unit area of apical plasma membrane are,

$$J_V^{am} = L_p^{am} \left\{ RT (C_{Na}^{cell} + C_K^{cell} + C_{Cl}^{cell} + C_A^{cell} + C_{Glu}^{cell} - C_{Na}^{lumen} - C_K^{lumen} - C_{Cl}^{lumen} - C_{Glu}^{lumen}) + (p^{lumen} - p^{cell}) \right\} \quad (8a)$$

$$J_V^{lm} = L_p^{lm} \left\{ RT (C_{Na}^{lis} + C_K^{lis} + C_{Cl}^{lis} + C_{Glu}^{lis} - C_{Na}^{cell} - C_K^{cell} - C_{Cl}^{cell} - C_A^{cell} - C_{Glu}^{cell}) + (p^{cell} - p^{lis}) \right\} \quad (8b)$$

$$J_V^{sm} = L_p^{sm} \left\{ RT (C_{Na}^{serosa} + C_K^{serosa} + C_{Cl}^{serosa} + C_{Glu}^{serosa} - C_{Na}^{cell} - C_K^{cell} - C_{Cl}^{cell} - C_A^{cell} - C_{Glu}^{cell}) + (p^{cell} - p^{serosa}) \right\} \quad (8c)$$

Water fluxes through membranes delimiting the lateral intercellular space from external solutions have to include reflection coefficients,

$$J_V^{tj} = L_p^{tj} \left\{ RT [\sigma_{Na}^{tj} (C_{Na}^{lis} - C_{Na}^{lumen}) + \sigma_K^{tj} (C_K^{lis} - C_K^{lumen}) + \sigma_{Cl}^{tj} (C_{Cl}^{lis} - C_{Cl}^{lumen}) + \sigma_{Glu}^{tj} (C_{Glu}^{lis} + C_{Glu}^{lumen})] + (p^{lumen} - p^{lis}) \right\} \quad (9a)$$

$$J_V^{ibm} = L_p^{ibm} \left\{ RT [\sigma_{Na}^{ibm} (C_{Na}^{serosa} - C_{Na}^{lis}) + \sigma_K^{ibm} (C_K^{serosa} - C_K^{lis}) + \sigma_{Cl}^{ibm} (C_{Cl}^{serosa} - C_{Cl}^{lis}) + \sigma_{Glu}^{ibm} (C_{Glu}^{serosa} + C_{Glu}^{lis})] + (p^{lis} - p^{serosa}) \right\} \quad (9b)$$

Rather than hydraulic conductance,  $L_p$ , in the text, we refer to osmotic permeability,  $P_f$ . With molar volume of water indicated by  $\bar{V}_W$ ,  $L_p$  and  $P_f$  are related by Finkelstein (1987),

$$P_f = \frac{RTL_p}{\bar{V}_W} \quad (10)$$

Mean valence of nondiffusible anions in the cell with concentration,  $C_A^{cell}$ , is denoted by  $z_A$ . Thus, the two electroneutrality conditions are given by:

$$C_A^{cell} = -(C_{Na}^{cell} + C_K^{cell} - C_{Cl}^{cell})/z_A \quad (14)$$

$$C_{Cl}^{lis} = C_{Na}^{lis} + C_K^{lis} \quad (15)$$

If  $I^{clamp}$  is the transepithelial clamping current and  $I_j$  is the current carried by  $j$  through the membrane indicated by superscript ( $j = Na^+$ ,  $K^+$ , or  $Cl^-$ ), the mathematical solution would have to obey the requirement:

$$I^{clamp} = I_{Na}^{am} + I_{Na}^{tj} + I_K^{am} + I_K^{tj} + I_{Cl}^{am} + I_{Cl}^{tj} \quad (16)$$

where  $I^{clamp} = 0$  ("open circuit") defines the mathematical solution containing the transepithelial potential difference.

## 2.4 Compliant Model and Volumes of Intraepithelial Compartments

For obtaining the hydrostatic pressure of the cell, we followed Weinstein and Stephenson (1979, 1981) and introduce a compliance model that assumes linear relationship between cell volume and cell pressure. If it is further assumed that the hydrostatic pressure of the cell adjusts itself to a value between ambient pressures weighted relative to the local compliant constants that are given the symbol  $\mu^m$ , we can write (Larsen et al. 2000),

$$p^{cell} = \frac{\mu^{am}}{\mu^{am} + \mu^{lm} + \mu^{sm}} p^{lumen} + \frac{\mu^{lm}}{\mu^{am} + \mu^{lm} + \mu^{sm}} p^{lis} + \frac{\mu^{sm}}{\mu^{am} + \mu^{lm} + \mu^{sm}} p^{serosa} \quad (17a)$$

Introducing relative compliance constants,

$$p^{cell} = \bar{\mu}^{am} p^{lumen} + \bar{\mu}^{lm} p^{lis} + \bar{\mu}^{sm} p^{serosa} \quad (17b)$$

With the volume of *lis* in the absence of fluid transport denoted,  $Vol^{lis,ref}$ , we have (Larsen et al. 2002):

$$Vol^{lis} = Vol^{lis,ref} [1 + \mu^{lm} (p^{lis} - p^{cell})] \quad (18)$$

$D^{cell}$  and  $M_A$  are number of cells per unit area of apical membrane and amount of nondiffusible anions per cell, respectively. Hence, cell volume is:

$$Vol^{cell} = D^{cell} M_A / C_A^{cell} \quad (19)$$

Here,  $C_A^{cell}$  belongs to dependent variables.

## 2.5 Electrical-Circuit Analysis

Shown in Fig. 1c, the five epithelial membranes constitute a bridge circuit. For convenience, in the Mathematica© equations below, the five membranes are indicated by  $am = 1$ ,  $sm = 2$ ,  $lm = 3$ ,  $tj = 4$ , and  $ibm = 5$ . The method used for calculating the transepithelial conductance (resistance) is as follows. Having chosen values for independent variables, the numerical solution provides all primary dependent variables. Integral conductances calculated as specified above are used to calculate the resistance of each of the five membranes,  $R_1 \dots R_5$ . Simulating a step change of the current  $\Delta I^{trans}$  through the circuit, Kirchhoff's rules are applied for setting up five simultaneous linear equations,

$$\begin{aligned}
I_1 R_1 + I_3 R_3 - I_4 R_4 &= 0 \\
I_3 R_3 + I_5 R_5 - I_2 R_2 &= 0 \\
I_2 + I_5 - \Delta I^{trans} &= 0 \\
I_1 - I_2 - I_3 &= 0 \\
I_4 - I_3 - I_5 &= 0
\end{aligned}$$

The currents flowing through the five resistors were obtained by using the solve routine of *Mathematica*©:

$$I_1 = -\frac{-(R_2 R_4 + R_3 R_4 + R_3 R_5 + R_4 R_5)}{R_1 R_2 + R_1 R_3 + R_2 R_3 + R_2 R_4 + R_3 R_4 + R_1 R_5 + R_3 R_5 + R_4 R_5} \Delta I^{trans}$$

$$I_2 = \Delta I^{trans} + \frac{(R_1 R_3 + R_2(R_1 + R_3 + R_4))}{-R_1 R_3 - R_1 R_4 - R_2(R_1 + R_3 + R_4) - R_5(R_1 + R_3 + R_4)} \Delta I^{trans}$$

$$I_3 = -\frac{(R_2 R_4 + R_1 R_5)}{R_1 R_2 + R_1 R_3 + R_2 R_3 + R_2 R_4 + R_3 R_4 + R_1 R_5 + R_3 R_5 + R_4 R_5} \Delta I^{trans}$$

$$I_4 = -\frac{-(R_1 R_2 - R_1 R_3 - R_2 R_3 - R_1 R_5)}{R_1 R_2 + R_1 R_3 + R_2 R_3 + R_2 R_4 + R_3 R_4 + R_1 R_5 + R_3 R_5} \Delta I^{trans}$$

$$I_5 = -\frac{(R_1 R_3 + R_2(R_1 + R_3 + R_4))}{-R_1 R_3 - R_3 R_4 - R_2(R_1 + R_3 + R_4) - R_5(R_1 + R_3 + R_4)} \Delta I^{trans}$$

The transepithelial electrical potential displacement  $\Delta V^{trans}$  and the resistance of the apical (luminal) membrane relative to the transcellular resistance are given by the relations,

$$\begin{aligned}
\Delta V^{trans} &= I_1 R_1 + I_2 R_2 \\
FR^{apical} &= I_1 R_1 / \Delta V^{trans}
\end{aligned}$$

Finally, the transepithelial conductance is calculated as  $G_t = \Delta I^{trans} / \Delta V^{trans}$ .

## 2.6 Nomenclature and Sign Conventions

Nomenclature is indicated in Fig. 1b and Appendix 1. The model comprises four well-stirred compartments: outside (luminal-) compartment (*o*), cell compartment (*cell*), lateral intercellular space (*lis*), and inside (serosal-, interstitial-) compartment (*i*). These are confined by five membranes: apical (*am*), serosal (*sm*), lateral (*lm*), tight junction (*tj*), and intercellular basement membrane (*ibm*). The primary

unknowns include cellular and paracellular concentrations of  $\text{Na}^+$ ,  $\text{K}^+$ , and  $\text{Cl}^-$ , glucose and nondiffusible intracellular anions, hydrostatic pressures in cell and *lis*, and electrical potentials in cell, *lis*, and outside compartment. Fluxes directed from lumen to cell and *lis*, from cell to serosa and *lis*, and from *lis* to serosa are positive. Electrical potentials are indicated with reference to serosal compartment ( $\psi^i \equiv 0$ ) so that the individual membrane potentials are given by  $V^{sm} = \psi^{cell} - \psi^i$ ,  $V^{lm} = \psi^{cell} - \psi^{lis}$ ,  $V^{am} = \psi^o - \psi^{cell}$ ,  $V^{ij} = \psi^o - \psi^{lis}$ , and  $V^{ibm} = \psi^{lis} - \psi^i$ .

### 2.7 Numerical Methods

The set of equations can be solved for both steady states and time-dependent states. In the general case, the transport equations for water and solutes are written as (Larsen et al. 2009):

$$\frac{d\bar{V}}{dt} = \sum_m J_{\bar{V}} \tag{20}$$

$$\frac{d(\bar{V} \cdot C_S)}{dt} = \sum_m J_S \tag{21}$$

where  $\bar{V}$  denotes the volume of cell or lateral intercellular space, and  $J_{\bar{V}}$  and  $J_S$  denote water and solute fluxes, respectively, through the various membranes, with  $m$  indicating membrane ( $m = 1-5$ ). In steady state, left hand side is zero. When transients are studied, time-dependent behavior of Eqs. (20) and (21) needs to be simulated. To solve the equations in time, we utilize second-order accurate, three-point backward difference schemes (Taylor expansion) as follows:

$$\frac{1}{2\Delta t} [3\bar{V}^{(n)} - 4\bar{V}^{(n-1)} + \bar{V}^{(n-2)}] = \sum_j J_{\bar{V}}^{(n)} \tag{22}$$

$$\frac{1}{2\Delta t} [3(\bar{V} \cdot C_S)^{(n)} - 4(\bar{V} \cdot C_S)^{(n-1)} + (\bar{V} \cdot C_S)^{(n-2)}] = \sum_m J_S^{(n)} \tag{23}$$

where index  $n$  refers to time  $t^n$  and  $\Delta t$  is the time step, such that  $t^n = t^{n-1} + \Delta t$ . Thus, the equations are solved for all variables with index  $n$  at time  $t = t^n$ , leaving the remaining terms as known from the former time steps. The equations are solved together with the above equations for electroneutrality and the compliance model. The strongly coupled nonlinear equations were solved to machine accuracy by a conventional iterative Newton-Raphson method. In forming the Jacobian matrix, the equations were not differentiated analytically as a simple difference scheme was employed. For analyses of transient states, the term ‘‘sampling frequency’’ refers to frequency of time steps. With a single time step, we jump directly from one steady state to another – skipping transient states.

## 2.8 Choice of Independent Variables

Appendix 2 lists independent variables of the model displayed in Fig. 1b. Ion permeabilities and maximum pump rates were chosen to obtain a net uptake of  $\text{Na}^+$  of about  $5,000 \text{ pmol cm}^{-2} \text{ s}^{-1}$  with associated volume absorption of 30–40  $\text{nL cm}^{-2} \text{ s}^{-1}$  together with intracellular concentrations and serosa-membrane potential in reasonable agreement with measured quantities (Windhager 1979). From measurements,  $C_{\text{Na}}^{\text{cell}} = 17.5$ ,  $C_{\text{K}}^{\text{cell}} = 113$ , and  $C_{\text{Cl}}^{\text{cell}} = 18 \text{ mM}$  at a serosal membrane potential of  $-76 \text{ mV}$  (Cassola et al. 1983; Edelman et al. 1978; Yoshitomi and Fromter 1985). The corresponding model values are given in Fig. 2. For simulating the somewhat low  $C_{\text{K}}^{\text{cell}}$ , we assumed a mean net charge of intracellular nondiffusible anions less than unity ( $z_A = -0.75$ ). In the model, the  $\text{Na}^+/\text{K}^+$  pump in the serosal plasma membrane is “silent” so that the active  $\text{Na}^+$  uptake is due entirely to the activity of lateral pumps (Kashgarian et al. 1985). The major electro-diffusive  $\text{K}^+$  exit from cells is through the  $\text{K}^+$  channels of *Im*. Both apical and “basolateral” plasma membrane domains contain water channels (Nielsen et al. 1996). The osmotic permeabilities were taken from experiments on rabbit proximal tubule (Carpi-Medina et al. 1984; Gonz ales et al. 1984). Solvent drag on sucrose indicated that the paracellular pathway of the kidney proximal tubule contributes to water transport across the epithelium (Whittembury et al. 1988), but the hydraulic conductance of tight junctions, which constitutes the rate limiting structure along the pathway, is not easy to determine. One would think that one way of doing this would be to block water channels of the apical membrane and measure the residual transepithelial water flux. This method was applied by Whittembury’s laboratory (Carpi-Medina and Whittembury 1988), and we have used the value thus estimated,  $P_{\text{osm}}^{\text{ij}} = 2.5 \times 10^3 \text{ } \mu\text{m s}^{-1}$ . As we shall see below, blocking the osmotic permeability of the apical membrane will lead to an increase in the osmolarity of *lis*, forcing an increased water flow along the paracellular pathway. Thus, our osmotic permeability of tight junctions is overestimated. However, as none of the conclusions, generally of semiquantitative nature, are affected by this choice, it is applied here in lack of better estimate. As emphasized above, the serosal plasma membrane contacting the epithelium’s basement membrane and the lateral plasma membrane constitute two separate domains. The model is born with similar transport systems in the two domains. The serosal-membrane fluxes governing the majority of computations were obtained by choosing small values of associated independent variables.

Molecular biological and biophysical studies indicated that paracellular fluxes are mediated both by cation and anion selective tight junction pores, recently reviewed by Fromm et al. (2017). Claudin-2 is selectively permeable for small cations like  $\text{Na}^+$  and  $\text{K}^+$  and permeable for water. Claudin-10a (and perhaps claudin-17) is selectively permeable for small anions like  $\text{Cl}^-$ . Reflection coefficients of tight junctions were taken from literature  $\sigma_{\text{Na}}^{\text{ij}} = \sigma_{\text{K}}^{\text{ij}} = 0.7$  and  $\sigma_{\text{Cl}}^{\text{ij}} = 0.45$  (Ullrich 1973). The interspace basement membrane is governed by physical properties of the basement membrane, and a morphometric study of rabbit proximal



tubule indicating that *ibm* constitutes 10% of the basement membrane area of the entire tubule (Welling and Grantham 1972; Welling et al. 1987a, b). Ion permeability of convection pores was selected to obtain the paracellular electrical resistance estimated by Frömter (1979) of about  $5 \Omega \text{ cm}^2$ , which requires a relatively high  $\text{Cl}^-$  permeability of delimiting membranes. The cation “selectivity” of the interspace basement membrane is that of free diffusion in water.

## 2.9 Geometrical Dimensions and Units of Physical Quantities

A stereological study of S1 segment of rabbit proximal tubule indicated an outer and inner diameter of 38 and 24  $\mu\text{m}$ , respectively, corresponding to a cell height of 7  $\mu\text{m}$ . Referring to 1 mm of tubule length, the following numbers were obtained: an epithelial volume of  $6.8 \times 10^5 \mu\text{m}^3$ , an apical membrane area of  $2.20 \times 10^6 \mu\text{m}^2$ , and a lateral membrane area of  $2.29 \times 10^6 \mu\text{m}^2$  (Welling and Welling 1988). With 300 cells per mm (Welling et al. 1987a), single-cell volume is about 2,267 fL. With gap junctions between cells, we assume that the epithelium constitutes a continuous functional syncytium.

Physical constants, independent variables, and computed dependent variables are in MKSA units. In the text, however, all variables are presented in units commonly used in physiological literature.

## 3 Results

### 3.1 General Features

Kidney proximal tubule accomplishes isosmotic transport in absence of glucose in luminal perfusion solution (Windhager et al. 1959; Morel and Murayama 1970). Figure 2 contains values given by the model for the reference state exposed to symmetrical external glucose-free solutions. With respect to cellular ion concentrations, it is noted that  $C_K^{cell}$  of 117 mM is fairly low, which is in agreement with measurements, recently reviewed by Weinstein (2013): 70 mM (Necturus), 113 mM (rat), and 68 mM (rabbit). The intracellular electrical potential,  $V^{cell} = -82 \text{ mV}$ , agrees with values measured in rat ranging between  $-64$  and  $-85 \text{ mV}$  (Frömter 1979). The lumen-negative transepithelial potential difference is no more than  $V^{trans} = -1.78 \text{ mV}$ , governed by high paracellular electrical conductance and the following transepithelial ion fluxes ( $\text{pmol cm}^{-2} \text{ s}^{-1}$ ):  $J_{Na} = 5,197$ ,  $J_K = 187$ , and  $J_{Cl} = 5,384$ . Fluxes through the apical membrane are associated with an apical membrane resistance of  $313 \Omega \text{ cm}^2$ , which is 57 times larger than the shunt resistance of  $5.5 \Omega \text{ cm}^2$ . The corresponding values for rat are 260 and  $5 \Omega \text{ cm}^2$ , respectively (Frömter 1982). At transepithelial osmotic equilibrium, water uptake would have

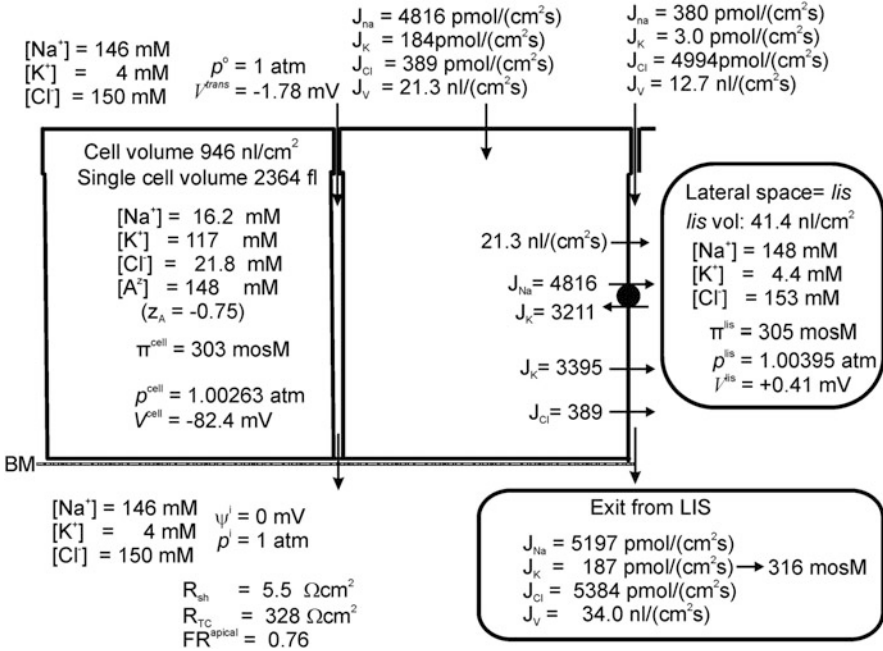


**Fig. 2** Reference state of the minimalistic model epithelium. With the large osmotic permeabilities estimated experimentally (Carpi-Medina et al. 1984; Gonzáles et al. 1984) is the fluid exiting the lateral intercellular space predicted to be hyperosmotic to bath: 316 mosM versus 300 mosM. Electrical resistances given by the model:  $R^{am} = 313 \Omega \text{ cm}^2$ ,  $R^{lm} = 15.9 \Omega \text{ cm}^2$ ,  $R^i = 4.43 \Omega \text{ cm}^2$ , and  $R^{bm} = 1.10 \Omega \text{ cm}^2$ .  $FR^{apical}$  is the ratio of apical (luminal) membrane resistance to transepithelial resistance

to be translateral, and with osmotic permeabilities obtained in experiments by Carpi-Medina and Whittembury (1988), the water uptake via apical membrane is  $21.3 \text{ nL cm}^{-2} \text{ s}^{-1}$ . This is about twice the water flux of  $12.7 \text{ nL cm}^{-2} \text{ s}^{-1}$  through tight junctions, which is driven by  $\Delta\pi = 5 \text{ mosM}$ . Convection fluxes energized by paracellular water absorption are discussed in detail below. Here it suffices to point out that paracellular solvent drag on potassium ions cannot account for transtubular  $K^+$  absorption which provides a  $K^+$  concentration of the absorbate that is significantly less than 1 mM; an estimate using numbers of Fig. 2 would give  $3.0 \text{ pmol cm}^{-2} \text{ s}^{-1} / 22.7 \text{ nl cm}^{-2} \text{ s}^{-1} = 0.24 \text{ mM}$ . This should be compared to the total  $K^+$  absorption that gives a  $K^+$  concentration of the absorbate of  $187/34.0 = 5.5 \text{ mM}$  (Fig. 2), that is, a value much closer to the 4 mM of the serosal bath. When glucose absorption is included, this number drops to  $[K^+]_{\text{absorbate}} = 190 \text{ pmol cm}^{-2} \text{ nl} / 46 \text{ nl cm}^{-2} = 4.1 \text{ mM}$ , see Fig. 4. Exit of water through the interspace basement membrane of low reflection coefficients is driven by a small hydrostatic pressure difference ( $p^{lis} - p^i$ ) of  $3.95 \times 10^{-3} \text{ atm}$ . With a total apical water uptake of  $J_V = 34.0 \text{ nL cm}^{-2} \text{ s}^{-1}$  at steady state, this is also the volume flux across *ibm*. The lateral intercellular space of an osmolarity of 305 mosM is no

more than 1.7% hyperosmotic relative to the symmetrical bathing solutions of 300 mosM. Nevertheless, the fluid exiting the lateral space of 316 mosM is 5.3% hyperosmotic with respect to bath. The difference in osmolarity between *lis* and the fluid emerging from *lis*, in this example 11 mosM, shows that exit fluxes are governed by relatively large electrodiffusion permeabilities of *ibm* (conf. Eq. 6), which exposes the unavoidable diffusion-convection problem of the exit pathway in isosmotic transport.

### 3.2 A Component of $\text{Na}^+$ Uptake Bypasses the Pump

Although the electrical driving force for  $\text{Na}^+$  movement through tight junctions is  $-2.19$  mV, the flux of  $\text{Na}^+$  of  $380 \text{ pmol cm}^{-2} \text{ s}^{-1}$  is inward showing that solvent drag overrules the electrochemical driving force of opposite direction. Formally, the  $\text{Na}^+$  current through tight junctions can be written,

$$I_{\text{Na}}^{\text{tj}} = G_{\text{Na}}^{\text{tj}} (V^{\text{tj}} - E_{\text{Na}}^{\text{tj}} + \Phi_{\text{Na}}^{\text{tj}}) \quad (24)$$

$G_{\text{Na}}^{\text{tj}}$  is the  $\text{Na}^+$  conductance of tight junctions,  $E_{\text{Na}}^{\text{tj}}$  the  $\text{Na}^+$  equilibrium potential across tight junctions,  $V^{\text{tj}}$  the transjunctional potential difference, and  $\Phi_{\text{Na}}^{\text{tj}}$  the driving force due to convection, which Ussing has given the expressive term “solvent drag.” In the electrodiffusion-convection regime, the term denoted  $\Phi_{\text{Na}}^{\text{tj}}$  of Eq. (24) is the driving force resulting from the convection process. Because we here consider an ion current, it follows that its dimension is “volt.” Ussing’s original mathematical treatment of solvent drag concerned unidirectional isotope fluxes of electroneutral molecules that included a hydrostatic pressure gradient as driving force for the net water flux. With this in mind, it should be evident that our treatment of solvent drag agrees with the original definition. Aiming at solvent drag:

$$\Phi_{\text{Na}}^{\text{tj}} = \frac{I_{\text{Na}}^{\text{tj}} - G_{\text{Na}}^{\text{tj}} (V^{\text{tj}} - E_{\text{Na}}^{\text{tj}})}{G_{\text{Na}}^{\text{tj}}}$$

There is strong dependence of  $\Phi_{\text{Na}}^{\text{tj}}$  on  $P_{\text{Na}}^{\text{tj}}$  (see Table 1). However, unlike paracellular transport, the overall tubule function is insensitive to a  $10\times$  decrease in  $P_{\text{Na}}^{\text{tj}}$ , which on the other hand leads to 11.3 times increase in paracellular solvent drag. Thus, even though the transepithelial potential difference is negative, our quantitative analysis predicts that solvent drag in tight junctions prevents passive back leak of  $\text{Na}^+$  to tubule lumen, which is contrary to information given in medical textbooks (Boron and Boulpaep 2017).

**Table 1** Solvent drag on sodium ions in tight junction

$P_{Na}^{ij}$ ( $\text{cm s}^{-1}$ )	$V^{trans}$ (mV)	$J_{Na}^{trans}$ ( $\text{pmol cm}^{-2} \text{s}^{-1}$ )	$J_V^{trans}$ ( $\text{nL cm}^{-2} \text{s}^{-1}$ )	$I_{Na}^{ij}$ ( $\mu\text{A cm}^{-2}$ )	$G_{Na}^{ij}$ ( $\text{mS cm}^{-2}$ )	$V^j$ (mV)	$E_{Na}^{ij}$ (mV)	$\Phi_{Na}$ (mV)
$1.25 \times 10^{-3}$	-1.78	5,195	34.0	36.70	6.65	-2.19	-0.40	7.3
$7.50 \times 10^{-4}$	-1.81	5,276	34.5	44.21	3.99	-2.23	-0.41	12.9
$3.75 \times 10^{-4}$	-1.83	5,336	34.9	49.99	1.99	-2.25	-0.42	27.0
$1.25 \times 10^{-4}$	-1.85	5,377	35.2	53.80	0.67	-2.28	-0.42	82.8

Independent model variables, except  $P_{Na}^{ij}$  (column 1), were kept at their standard value. The computed paracellular solvent drag on sodium ions is listed in last column. It shows that there is a strong inverse dependence of  $\Phi_{Na}^{im}$  on  $P_{Na}^{ij}$ . On the other hand, this has little effect on the overall tubule function as exemplified by the transepithelial  $\text{Na}^+$  and water fluxes and the transepithelial potential difference.

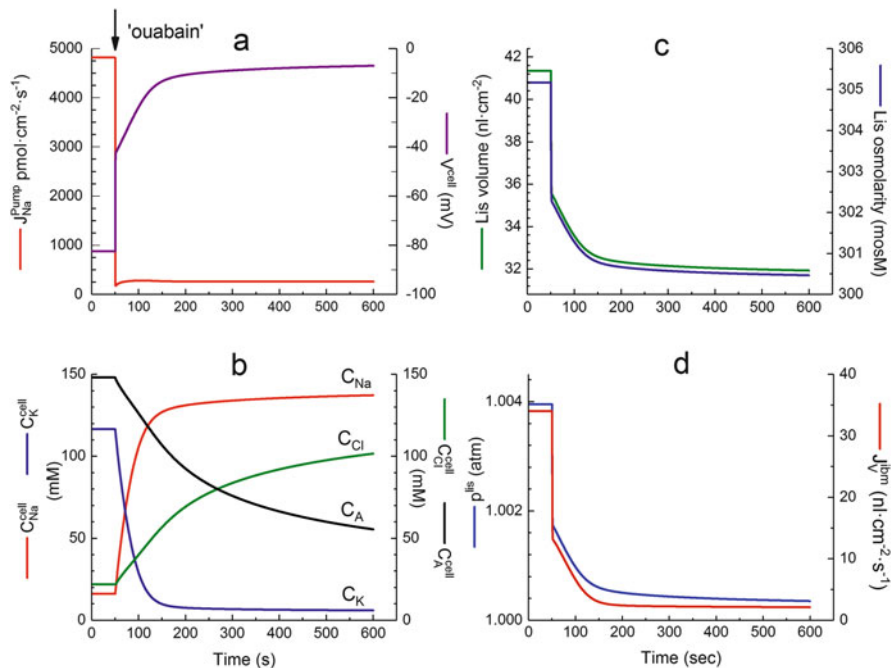


**Fig. 3 (a–d)** Effects of inhibition of the  $\text{Na}^+\text{-K}^+\text{-ATPase}$  of lateral membrane. **(a)** at time = 50 s, maximum pump flux (Eq. 4a) was reduced exponentially ( $\tau = 0.1$  s, Eq. 25) by a factor of  $50\times$ . This resulted in fast drop of  $J_{\text{Na}}^{\text{pump},lm}$  and an associated fast cell depolarization of 40 mV. The further slow depolarization owes to dissipation of ion gradients at rates given by respective membrane permeabilities and cellular ion pool sizes. **(b)** Cation-gradient dissipations lead to  $\text{Na}^+$  and  $\text{Cl}^-$  accumulation and  $\text{K}^+$  loss. The net effect is cell swelling as indicated by the decrease in concentration of nondiffusible intracellular anions ( $C_A$ ). **(c)** As consequence of the arrest of lateral active  $\text{Na}^+$  flux and subsequent slow ion-gradient dissipations, volume and osmolarity of *lis* decrease accordingly. **(d)** The associated drop in hydrostatic pressure directs reduced exit of fluid across the interspace basement membrane

### 3.3 Inhibition of the $\text{Na}^+/\text{K}^+$ Pump

The lateral  $\text{Na}^+/\text{K}^+\text{-ATPase}$  energizes ion and water fluxes through the epithelium (Garg et al. 1981; Gyory and Kinne 1971), and owing to the very high expression of the enzyme in proximal tubule (Jørgensen 1986), pump currents may have significant electrophysiological and hydrodynamic effects. Inhibiting the  $\text{Na}^+/\text{K}^+$  pump by a  $50\times$  reduction of  $P_{\text{Na}^+,\text{K}^+}^{lm,pump}$  (Eq. 4a) is shown in Fig. 3. The time course of inhibition is given by,

$$c(t) = c(\infty) - (c(0) - c(\infty))\exp(-t/\tau), \quad (25)$$

Here,  $c(0)/c(\infty) = 50$  and  $\tau = 0.1$  s. Due to the voltage dependence of the pump current, the instantaneous membrane depolarization is fast and large. Computations

given by the model (Fig. 3a) predict an ouabain-induced cell depolarization of 40 mV for a pump current of  $155 \mu\text{A cm}^{-2}$ . This is to be compared to a pump-generated hyperpolarization of 15–20 mV of the inward facing membrane of frog skin for pump currents of  $40\text{--}50 \mu\text{A cm}^{-2}$  (Nagel 1980), and a 1.8 mV hyperpolarization of giant axon caused by a pump current of  $1.8 \mu\text{A cm}^{-2}$  (Hodgkin and Keynes 1955). Our conclusion here is that the contribution of the pump current to the membrane potential has evolved for serving tissue specific functions of the  $\text{Na}^+/\text{K}^+$  pump; in proximal tubule, the pump serves the returning of a large volume of isosmotic fluid to the extracellular fluid which requires high activity of the  $\text{Na}^+/\text{K}^+$ -ATPase. In the skin of frogs on land the function of the sodium pump is to return  $\text{Na}^+$  (and  $\text{Cl}^-$ ) to the body fluids during evaporative water loss from the cutaneous surface fluid generated by subepidermal mucous glands (Larsen 2011). Finally, electrical signalling in excitable cells relies on the membrane potential being uniquely given by the ratio of the membrane's  $\text{Na}^+$  and  $\text{K}^+$  permeabilities (Hodgkin 1958), which presupposes relatively very low activity of the  $\text{Na}^+/\text{K}^+$ -ATPase. Secondary to the voltage dependent sudden decrease, the pump flux decreases further but with a longer time constant caused by the relatively slow redistribution of cellular cation pools (Fig. 3b). With negatively charged intracellular macroions, the working of the pump keeps the cell from swelling and bursting, which otherwise would take place due to the continuous inflow of  $\text{Na}^+$  (and  $\text{Cl}^-$ ), conf. the theory of Gibbs-Donnan equilibrium (Sten-Knudsen 2002). Thus, concomitant with accumulation of cellular  $\text{Na}^+$  and  $\text{Cl}^-$ , the cell swells (Fig. 3b). The sudden reduction in pumping of  $\text{Na}^+$  into the lateral intercellular space and the slow cellular ion gradient dissipations result in reduction in osmolarity and volume of *lis* that takes place with similar fast and slow time courses (Fig. 3c). The coupling of the pump flux and the water flow across the lateral membrane as indicated in Fig. 3c is discussed in detail in Sect. 3.5. The rate of exit of fluid into the serosal compartment is governed by the hydrostatic pressure difference between the lateral intercellular space,  $p^{lis}$ , and serosal compartment,  $p^i$  of 1 atm (Fig. 3d).

### 3.4 Effect of Adding Glucose

Sodium and water absorption increase significantly together with apical membrane depolarization if organic solutes are added to the tubular perfusion solution (Lapointe and Duplain 1991). In rabbit and rat proximal convoluted tubules, significant effects on the rate of fluid absorption were observed upon removal of luminal glucose and other metabolites (Burg et al. 1976; Frömter 1982). We have chosen values of independent variables governing apical  $\text{Na}^+$  uptake (Eqs. 1a–3a) for reproducing studies simulating the abovementioned significant effects of glucose. Thus, in the following, fluxes carried by Eq. (3a) are significant as compared to fluxes generated by Eqs. (1a) and (2a). The computed steady state with the physiological concentration of 5 mM glucose is shown in Fig. 4. The pertinent findings can be summarized. In steady state, the cellular glucose concentration is about twice that of the external concentration. Compared to Fig. 2 with no glucose,  $C_{\text{Na}}^{cell}$  is increased while  $C_{\text{K}}^{cell}$  is decreased, leading to 3% cell swelling from 2,366 to 2,436 fL. Such a

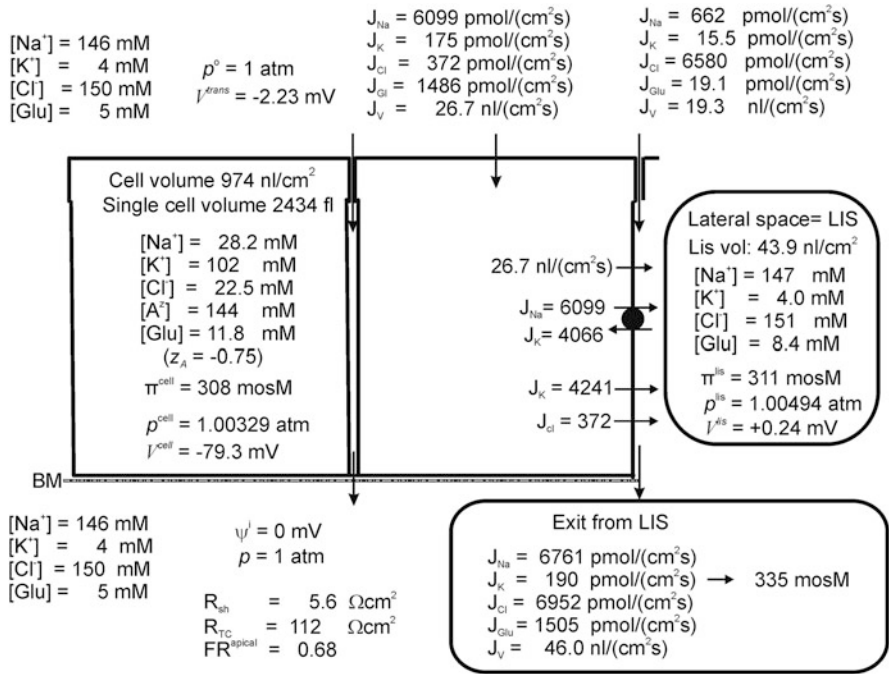


**Fig. 4** The model epithelium engaged in glucose absorption. The glucose uptake across the luminal membrane is coupled to uptake of sodium ions and driven by the electrochemical gradient for  $Na^+$  (SGLT2, Eq. 3a). Therefore, addition of glucose to external baths results in stimulation of the active  $Na^+$  flux across the lateral membrane from 4,816 (Fig. 2) to 6,099  $\text{pmol cm}^{-2} \text{ s}^{-1}$ . The enhanced lateral  $Na^+$  pump flux increases the  $Na^+$  concentration and osmolarity of the lateral intercellular space, which in turn increases transepithelial fluid uptake, from 30 to 46  $\text{nL cm}^{-2} \text{ s}^{-1}$ . Importantly, this results in an increase in the hyperosmolarity of transported fluid, from 316 to 335 mosM. Electrical resistances given by the model:  $R^{am} = 96.5 \Omega \text{ cm}^2$ ,  $R^{lm} = 17.3 \Omega \text{ cm}^2$ ,  $R^j = 4.45 \Omega \text{ cm}^2$ , and  $R^{ibm} = 1.10 \Omega \text{ cm}^2$

small cell volume change indicates a priori an insignificant increase in intracellular chloride concentration, which is confirmed quantitatively by numbers given by the model,  $C_{Cl}^{cell} = 21.8$  and  $22.5 \text{ mM}$ , respectively. The glucose-induced hyperpolarization of the transepithelial potential difference of  $-0.45 \text{ mV}$  from  $-1.78$  to  $-2.23 \text{ mV}$ , compare Fig. 2 with Fig. 4, is comparable in absolute magnitude to that of rat proximal tubule,  $-0.36 \pm 0.22 \text{ mV}$ , mean  $\pm$  S.D. (Frömter 1982). In the same study, Frömter perfused rat tubule in situ with Ringer’s solution containing 30 mM bicarbonate in the perfusion solution. Prior to glucose, the transepithelial potential difference was lumen positive but becoming lumen negative, as predicted by model computation, when perfused with 3 mM glucose. The stimulated sodium pump flux results in increased osmolarity of *lis* together with an increased water uptake from 34 to 46  $\text{nL cm}^{-2} \text{ s}^{-1}$ . The deviation ( $\Delta$ ) from isosmotic transport becomes significantly larger following addition of glucose, i.e.,  $\Delta = 16 \text{ mosM}$  and  $\Delta = 29 \text{ mosM}$  as indicated in Figs. 2 and 4. The increased fluid uptake discussed above includes an increased flow of fluid in tight junctions, from 12.7 to

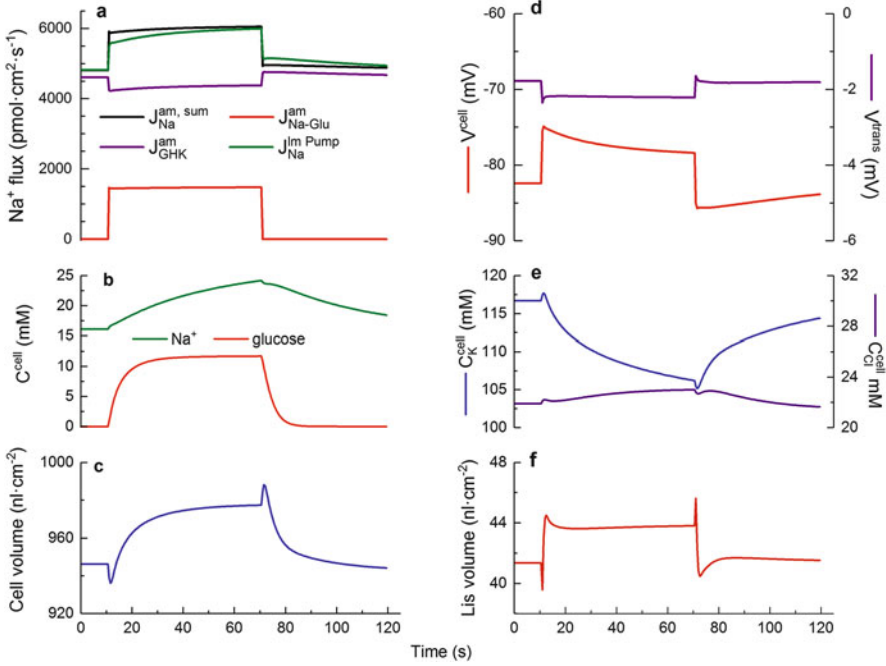


**Fig. 5 (a–f)** Effects of reversible bilateral exposure of 5 mM glucose of 60 s duration. **(a)** Fluxes carried by electrogenic Na<sup>+</sup> pathways  $J_{Na}^{am, sum} = J_{GHK}^{am} + J_{Na-Glu}^{am}$ . Note initial decrease in GHK-flux caused by depolarization of apical membrane.  $J_{Na}^{pump, lm}$  is stimulated “instantly” and secondarily as a consequence of a slow increase in  $C_{Na}^{cell}$ . See text for discussion. **(b)** Inflow of Na<sup>+</sup> and glucose results in cellular accumulation of the two solutes, but steady state is not achieved for Na<sup>+</sup> within the 60-s glucose pulse. **(c)** Cell swelling due to accumulation of Na<sup>+</sup> and glucose is preceded by fast volume decrease caused by the osmotic effect of adding glucose. **(d)** The electrogenic nature of the apical Na-glucose transporter is reflected in significant membrane depolarization and associated small hyperpolarization of  $V^{trans}$ . **(e)**  $C_K^{cell}$  decreases with long time constant, e.g., at steady state is  $C_K^{cell} = 102$  mM (Fig. 4), while increase in  $C_{Cl}^{cell}$  is modest. **(f)** The relatively small *lis* volume responds near instantly to adding/removing glucose to external compartments that embrace the steady volume increase caused by an increase in  $C_{glucose}^{lis}$  to 8.4 mM (Fig. 4)

$19.3 \text{ nL cm}^{-2} \text{ s}^{-1}$ , which results from increased osmolarity of *lis* from 305 to 311 mosM. Due to convection, this has direct effect on cation fluxes in tight junctions; e.g., for  $P_{Na}^{ij} = 1.25 \times 10^{-3} \text{ cm s}^{-1}$  is  $J_{Na}^{ij}$  increased from 380 to 662 pmol  $\text{cm}^{-2} \text{ s}^{-1}$ . The number of 662 pmol  $\text{cm}^{-2} \text{ s}^{-1}$  obtained with glucose in luminal solution is probably the better estimate of the paracellular Na<sup>+</sup> reabsorption driven by solvent drag in proximal convoluted tubule.

In Fig. 5 are shown time-dependent states induced by 60-s bilateral exposure to 5 mM-glucose. By choosing  $\tau = 0.1 \text{ s}$  (Eq. 25), the time course of cell variables given in Fig. 5 is reflecting characteristic times of intracellular pools of the “functional syncytium.” Due to the electrogenic nature of the apical Na<sup>+</sup>-glucose transporter (Eq. 3a), the cell membrane potential depolarizes by 7 mV (Fig. 5d), which is comparable to  $5.7 \text{ mV} \pm 2.0$  in rat (Frömter 1982). In the same study,



Frömter found that the resistance of the brush border membrane decreased to  $52.8 \pm 12\%$  (mean  $\pm$  SD) of its control value. In the model, apical membrane resistance dropped from 313 to  $96 \Omega \text{ cm}^2$ , i.e., to 31% of the control value. A plausible reason for the difference between experiment and computation is that Frömter had 3 mM glucose in the luminal perfusion solution as compared to our 5 mM glucose (Eq. 3a). Thus, with 3 mM glucose, the computed apical membrane resistance dropped to 46% of the control value which is within the abovementioned experimental range (details not shown). As a novel result, it should be noted that the addition of glucose also leads to “instantaneous” increase in  $J_{Na}^{lm,pump}$  (Fig. 5a, green graph) which is the consequence of the pump current being an instantaneous function of lateral membrane potential (Eq. 4a). The effect of activating rheogenic  $\text{Na}^+$  uptake across the apical membranes on  $\text{Na}^+$  pumping rate at the lateral membrane and the associated enhanced rate of fluid uptake constitute a mechanism of “cross-talk” that is not described before. The depolarization is about the same for apical and lateral membranes, because the cell is “short-circuited” by the low-resistance paracellular shunt, cf. time course of  $V^{trans}$  shown in Fig. 5d. Subsequently,  $J_{Na}^{lm,pump}$  increases slowly governed by slow increase in  $C_{Na}^{cell}$  (Fig. 5b).

The cell depolarization indicated in Fig. 5d decreases the  $\text{Na}^+$  flux in apical GHK-rectifying  $\text{Na}^+$  channels, conf. Eq. (1a) (Fig. 5a purple graph). In recordings of the total membrane current, this would be masked by the larger  $\text{Na}^+$  flux via the  $\text{Na}^+$ -glucose transporter (Fig. 5a). The decrease in  $C_K^{cell}$  from 116 to 106 mM (Fig. 5e), concomitant with the increase in  $C_{Na}^{cell}$ , should be compared with the small cell swelling mentioned above, which by and large is caused by the accumulated electroneutral glucose (Fig. 5b, e). This conclusion is in agreement with microscopically observed cell volume changes in microperfused proximal convoluted tubule of rabbit kidney (Burg et al. 1976).

In conclusion, the model reproduces measured glucose effects on  $\text{Na}^+$  fluxes, electrophysiology, and cell volume. Besides stimulated transepithelial  $\text{Na}^+$  and glucose fluxes fluid uptake as well is increased. It is noteworthy that the solute-coupled fluid flux is predicted to become more hyperosmotic when the proximal kidney tubule is engaged in glucose reabsorption, i.e., 316 mosM versus 335 mosM, which should be compared to “bath” osmolarities of 300 and 305 mosM, respectively.

### 3.5 Blocking Water Channels of Apical Membrane

Reducing the osmotic permeability of the apical membrane from  $0.449 \times 10^4$  to  $0.449 \mu\text{m s}^{-1}$  results in elimination of translateral water flow with hardly detectable effects on rate of active  $\text{Na}^+$  uptake and overall transepithelial water absorption, the latter being 34.0 and 35.5  $\text{nL cm}^{-2} \text{ s}^{-1}$ , respectively (Figs. 2 and 6). At the new steady state with little change in apical flux of sodium ions, the pumping of  $\text{Na}^+$  into *lis* is also changed by a small amount by the above maneuver,  $J_{Na}^{lm,pump} = 4,816$  and 4,837  $\text{pmol cm}^{-2} \cdot \text{s}^{-1}$ , respectively (Figs. 2 and 6). Water is now forced to take the paracellular route. Osmolarity and hydrostatic pressure of *lis*, governing entrance

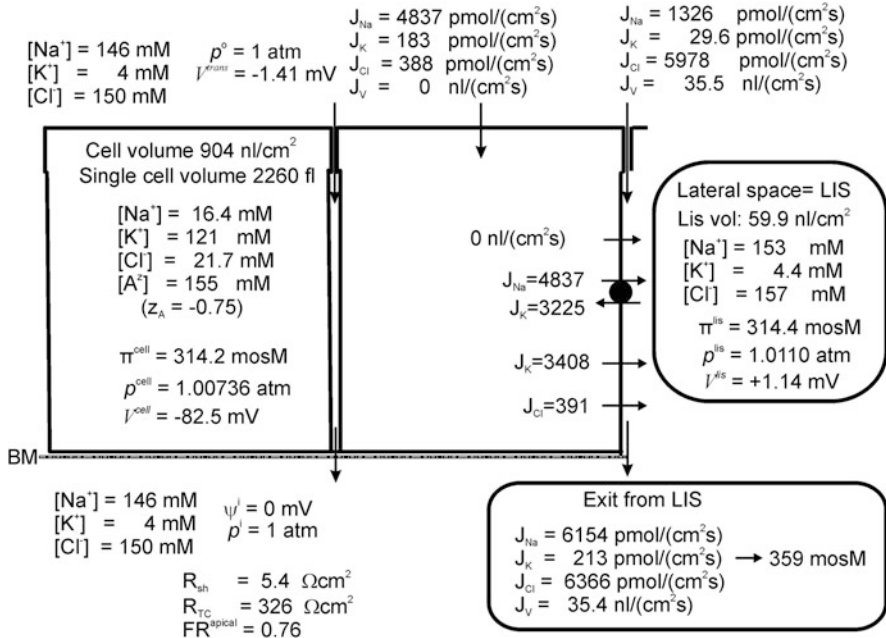


**Fig. 6** Steady-state solution with eliminated apical osmotic permeability. Apical  $P_f$  was reduced by a factor of  $10^4$  from  $0.449 \times 10^4$  to  $0.449 \text{ } \mu\text{m s}^{-1}$ . At transepithelial osmotic equilibrium, this eliminates cellular water transport, thus simulating AQP-1 (—/—). Electrical resistances given by the following models:  $R^{\text{am}} = 312 \text{ } \Omega \text{ cm}^2$ ,  $R^{\text{lm}} = 14.3 \text{ } \Omega \text{ cm}^2$ ,  $R^{\text{ij}} = 4.37 \text{ } \Omega \text{ cm}^2$ , and  $R^{\text{bbm}} = 1.08 \text{ } \Omega \text{ cm}^2$ . It is important to note that the transepithelial water flux is not significantly reduced by eliminating the apical membrane's water channels,  $J_V^{\text{bbm}} = 34.0$  and  $35.4 \text{ nL cm}^{-2} \text{ s}^{-1}$ , respectively (Figs. 2 and 5)

and exit of water across tight junction and interspace basement membrane, respectively, energize the significantly increased water flux along the paracellular route. The larger ion concentrations of *lis* result in increased convection-electrodifusion fluxes through *ibm* as reflected in the increased osmolarity to  $359 \text{ mosM}$  of the fluid emerging from *lis* (Fig. 6).

The relationships described above can be analyzed in detail by inspecting time-dependent states following a mono-exponential reduction of  $P_f^{\text{am}}$  from  $0.449 \times 10^4$  to  $0.449 \text{ } \mu\text{m/s}$  governed by  $\tau = 1 \text{ s}$  (Eq. 25); see Fig. 7a–f. The initial response to “eliminating” the apical water permeability is a shift of water volume from cells to *lis* driven by the difference in osmolarity between the two compartments, which is maintained by pumping of  $\text{Na}^+$  into *lis* (Fig. 7a). In the beginning, where volume shift is fast,  $C_{\text{Na}}^{\text{cell}}$  increases rapidly, whereby the  $\text{Na}^+$  pump flux is transiently stimulated (Fig. 7b). This lasts for about 20 s, where the osmolarity of *lis* of a relatively small volume increases toward its new steady-state value. While  $C_{\text{Cl}}^{\text{cell}}$  increases transiently, the concentration of nondiffusible anions increases in parallel with loss of cell volume (Fig. 7c). The increase in osmolarity of *lis* drives fluid into *lis* from the luminal solution (Fig. 7d), which brings ions into the compartment by solvent drag (Eq. 6). At the beginning of *lis*-volume expansion,  $p^{\text{lis}}$  is too low for

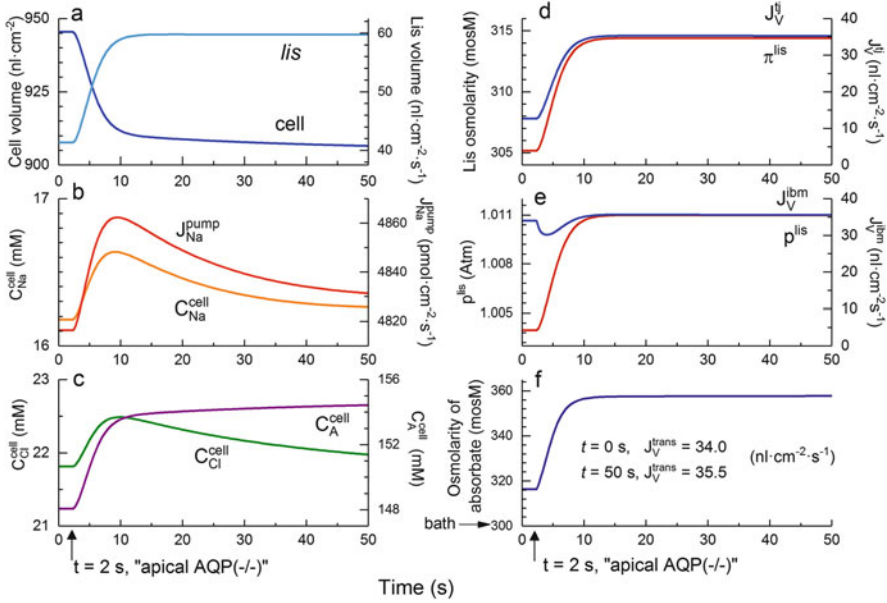


**Fig. 7 (a–f)** Time course of physiological variables in response to “eliminating” osmotic permeability of apical membrane. At time = 2 s and governed by  $\tau = 1$  s,  $P_f^{am}$  was reduced exponentially from 4,490 to 0.449  $\mu\text{m s}^{-1}$ . **(a)** this results in a fast shift of water volume from cells to *lis*. **(b)**  $C_{Na}^{cell}$  increases transiently, which stimulates  $\text{Na}^+$  pump flux,  $J_{Na}^{pump,lm}$ . **(c)** While the transient increase in  $C_{Cl}^{cell}$  parallels the transient increase in  $C_{Na}^{cell}$ , the increase in concentration of nondiffusible anions is closely following the loss of cell volume. **(d)** The water flux is redirected from being translateral to being paracellular driven by the increased osmolarity of *lis* governed by the  $C_{Na}^{cell}$ -stimulated increase in  $J_{Na}^{pump,lm}$ . **(e)** Due to inflow of water, the hydrostatic pressure of *lis* increases, which drives the volume flux across the interspace basement membrane  $J_V^{ibm}$ . **(f)** The final result is a significant increase in osmolarity of the fluid emerging from *lis* due to convection-electrodiffusion of solutes across the interspace basement membrane (Eq. 6). Notably, at the new steady state, the transepithelial water flux is about the same as the water flux prior to eliminating  $P_f^{am}$  (35.5 versus 34.0  $\text{nL cm}^{-2} \text{s}^{-1}$ )

preventing a decrease in the flux of fluid across *ibm*,  $J_V^{ibm}$ , conf. Eq. (9b) (Fig. 7e). This is transient, however; the continued influx of fluid across tight junction causes  $p^{lis}$  to increase, which enhances the fluid efflux across *ibm* into the serosal compartment. The new steady state is reached when  $J_V^{ibm}$  matches  $J_V^{lm}$  (Fig. 7e,  $J_V^{lm} = 0$  at all times). The significantly increased solute concentrations of *lis* combined with relatively large ion diffusion permeabilities of *ibm* (Eq. 6) causes the osmolarity of the fluid exiting the epithelium to increase to 359 mosM, which now becomes hyperosmotic by 59 mosM.

With isosmotic luminal perfusate and bath solutions, Schnermann et al. (1998) found that the fluid absorption rate in the S2 portion was halved in AQP-1 knock-out [−/−] mice; expressed in nL per mm tubule length, the rate dropped from  $0.64 \pm 0.15$  (wild type,  $n = 8$ ) to  $0.31 \pm 0.12$  (−/−,  $n = 5$ ). Our analysis presented

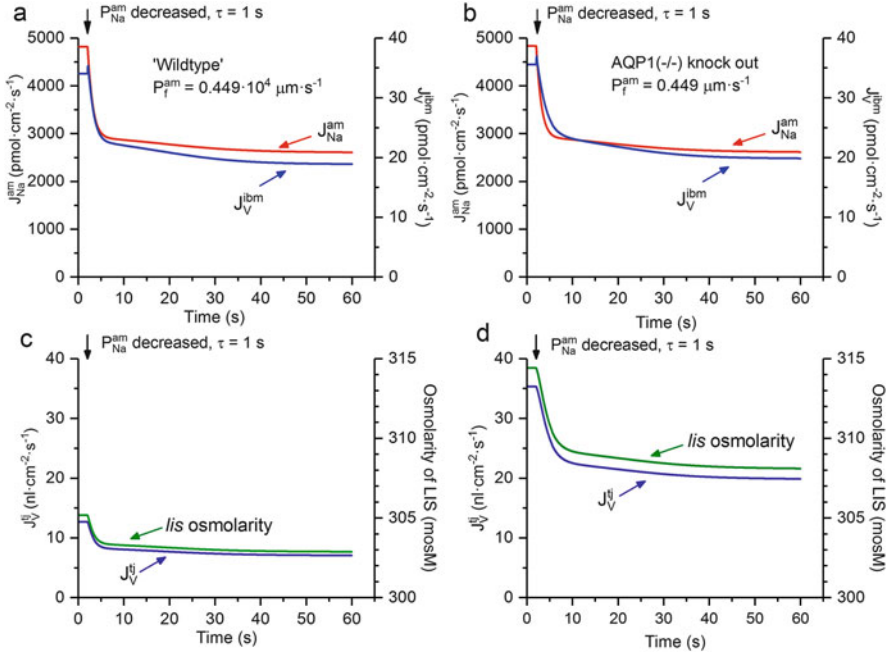


**Fig. 8 (a–d)** Effects of reducing apical  $P_{Na}$  on water fluxes. Reducing apical entrance permeability of sodium ions ( $\tau = 1$  s, text Eq. 25) results in parallel decreases in  $\text{Na}^+$  flux and rate of transepithelial water absorption. This response is independent of the pathway taken by water. (a) Water absorption is both translateral and transjunctional. (b) About similar responses are seen after having reduced apical osmotic permeability. (c) In “wild type” with intact osmotic permeability of the apical membrane, the small paracellular water uptake is driven by a relatively small difference in osmolarity between surrounding solutions of 300 mosM and *lis*. (d) With the translateral water uptake eliminated, all of the water enters the epithelium through tight junctions, which requires larger osmotic driving force

above showed that a very significant reduction in the number of water channels of the luminal membrane effectively eliminated cellular water fluxes but did not per se reduce the transepithelial absorption of water when studied at transepithelial osmotic equilibrium, where the rate of transepithelial water uptake as found by Solomon’s group (Windhager et al. 1959) is being directed by the rate of active  $\text{Na}^+$  uptake. Therefore, it might well be that the observed significant reduction in fluid absorption in AQP-1(-/-) mice observed by Schnermann et al. (1998) would have to be ascribed to the authors’ concomitantly reported reduction in active  $\text{Na}^+$  absorption. For testing this hypothesis, we studied the effect of reducing the rate of  $\text{Na}^+$  absorption on transtubular water absorption; see Fig. 8. Wild type and AQP-1 knock-out show similar reduction in rate of fluid uptake in response to reduction in the rate of transepithelial  $\text{Na}^+$  uptake, here expressed as volume flow out of *lis*, cf. the time course of  $J_V^{ibm}$  in Fig. 8a, b. The transepithelial water flow in Fig. 8b is entirely paracellular so the lack of translateral water uptake is reflected in an increased transjunctional water flux and osmolarity of *lis*, compare Fig. 8d with Fig. 8c.

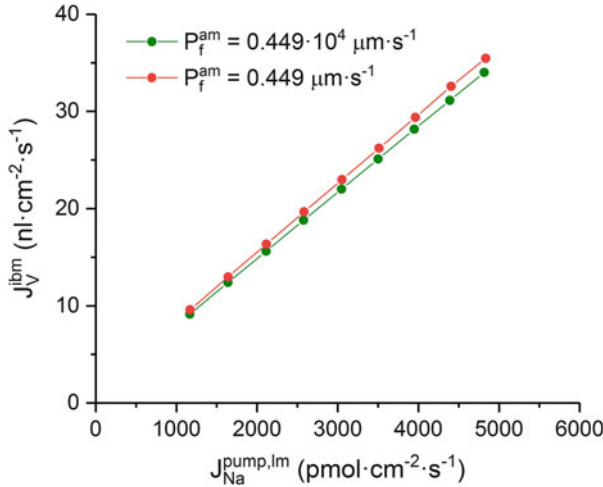


**Fig. 9** The fundamental dependence of rate of water absorption on lateral active  $\text{Na}^+$  flux. The rate of water absorption is governed by the rate at which  $\text{Na}^+$  ions are pumped into the lateral intercellular space independently of the pathway taken by water, mostly translateral (red) or purely transepithelial (green)

The decisive influence on water absorption of the rate of active  $\text{Na}^+$  flux across the lateral membrane is well documented by the computed relationships between transepithelial water uptake and the rate of pumping of  $\text{Na}^+$  into the lateral space in wild type and apical AQP-1 knock-out, respectively; see Fig. 9.

### 3.6 Volume Response of the Epithelium to a Luminal Osmotic Pulse

Exposure of the epithelium to a luminal hyperosmotic pulse results in reversible cell shrinkage (Fig. 10a, b). This is similar to rabbit proximal straight tubule, which does not exhibit volume regulatory increase (Kirk et al. 1987). Volume of the lateral intercellular space increases (Fig. 10c), reflecting that the influx of water from cells to *lis* exceeds the efflux of water to luminal bath through tight junctions. The explanation for this is obvious: the osmotic water permeability of apical and lateral plasma membranes is larger than that of tight junctions; there is, therefore, a flow of water from cells to *lis*, which swells. The loss of cell volume is quantitatively reflected in the increase in concentration of nondiffusible anions (Fig. 10d), a principle that was applied by Reuss (1985) for real-time monitoring of volume changes of epithelial cells in studies of cell volume regulation. The transient increase in osmolarity of cells and *lis* follows the external osmotic pulse in such a way that *lis* remains hyperosmotic to cells at all times maintained by lateral  $\text{Na}^+/\text{K}^+$  pump (Fig. 10e, f).

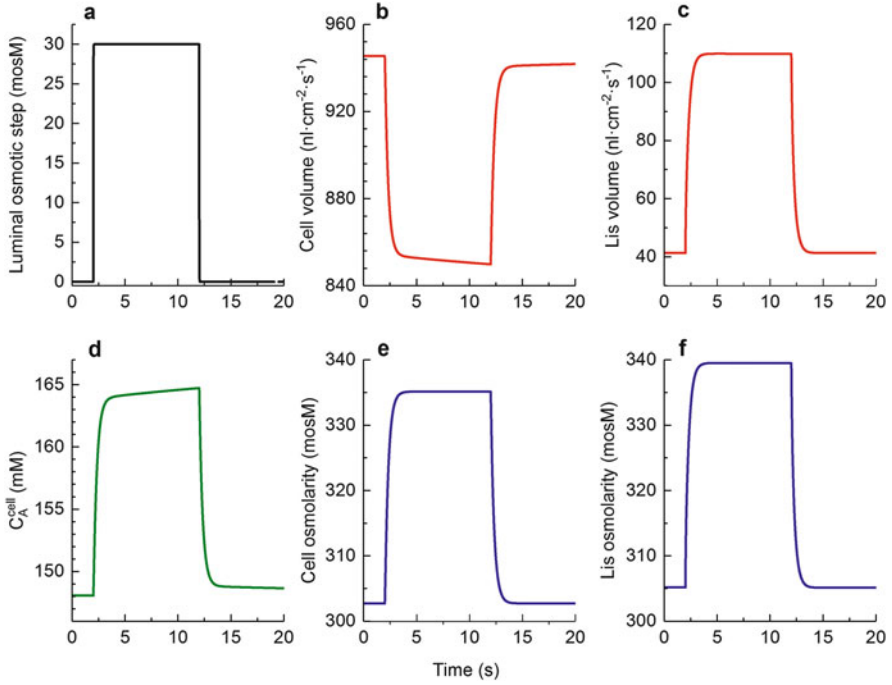


**Fig. 10** (a–f) Time-dependent responses to reversible luminal osmotic step. (a) Pulse of 30-mosM of an electroneutral, non-permeable solute applied to outside (luminal) solution. (b, c) Time course of change in the two intraepithelial water volumes; cell volume decreases, while *lis* volume increases. (d) The loss of cell water results in concentration increase in the non-permeable negatively charged intracellular electrolyte with a time course similar to that of change in cell volume. (e, f) Cell and *lis* osmolarity increase. At all times is osmolarity of *lis* larger than osmolarity of cell

### 3.7 Uphill Water Transport and Intraepithelial Water Fluxes

In Fig. 11, a non-permeable electroneutral solute is added in steps of 5 mosM to the luminal compartment. The two examples are with and without 5 mM glucose, respectively. In both cases, the relationship between water fluxes emerging from the lateral intercellular space and osmotic driving force is near-linear, displaying x-axis intercepts of  $-27$  and  $-37$  mosM, respectively. Thus, the model reproduces “uphill” water transport as observed in proximal tubule of rat (Green et al. 1991) and mice (Schnermann et al. 1998) and generated by previous models of leaky epithelia (Weinstein and Stephenson 1981; Larsen et al. 2000, 2009). In the literature, an (apparent) osmotic permeability of the epithelium is calculated by:

$$P_f^{epit} = \Delta J_V^{trans} / (\Delta \pi^o \cdot \bar{V}_W),$$

where  $\bar{V}_W = 18.1 \text{ cm}^3/\text{mol}$  is the molar volume of water at 310 K. From the slope of linear fits,  $P_f^{epit} = 680 \text{ } \mu\text{m s}^{-1}$ . This is significantly smaller than

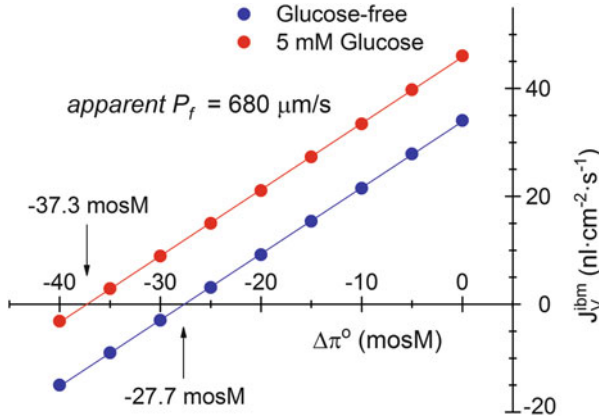


**Fig. 11** The model epithelium transports water against an adverse osmotic gradient (“uphill”). A ramp of increasing outside concentration of a non-permeable electroneutral solute,  $\Delta\pi^o$ , was imposed on the model epithelium. The graph shows computed *steady-state* water fluxes emerging from the lateral intercellular space at each ramp step of 5 mosM. The enhanced water flux following addition of glucose owes to the coupling of  $\text{Na}^+$  and glucose in apical SGLT2 which depolarizes the cell membranes. As a result, the  $\text{Na}^+$  pumps in the lateral membrane are stimulated (“cross-talk”) which directs an enhanced rate of transepithelial water uptake. Full lines are linear fits to computed points. The slope of the linear relationships denoted *apparent*  $P_f$  has physical dimension of osmotic permeability. In the literature, it is used as measure of the osmotic permeability of the epithelium. As discussed in the text, its physical significance is ambiguous with no relationship to an osmotic permeability and should be abandoned

the rate-limiting osmotic permeabilities of apical entrance pathways,  $P_f^{am} + P_f^{tj} = 4,490 + 2,500 = 6,990 \mu\text{m s}^{-1}$ . To explain this discrepancy, we will study non-stationary water fluxes between intraepithelial compartments by model computations, which cannot be studied by experiment. Figure 12 depicts the response of the apical membrane water flux to a 30 mosM pulse applied to luminal compartment. Prior to the pulse, the water flux is  $21.3 \text{ nL cm}^{-2} \text{ s}^{-1}$ . The “instantaneous” response is a fast reversal of the water flux to  $-197 \text{ nL cm}^{-2} \text{ s}^{-1}$ , driven by the imposed osmotic pulse, followed by relaxation toward an inward stationary flux of  $35.1 \text{ nL cm}^{-2} \text{ s}^{-1}$  at the end of the pulse. While this inward water flux is energized by ATP hydrolysis at the lateral  $\text{Na}^+/\text{K}^+$  pumps, the time course of the relaxation depends on the compliance of the lateral plasma membrane; the more resilient the membrane, the longer it takes to achieve the new stationary flux, and for large  $\mu^{lm}$ , the water flux response is heavily attenuated as compared to the squared shape of the osmotic pulse. The standard compliance constant of the lateral membrane,  $\mu^{lm} = 2.5 \times 10^{-3} \text{ Pa}^{-1}$ , is taken from experiments on *Necturus* gallbladder (Spring and Hope 1978). As seen, this gives rise to transients of a few seconds duration. At the prevailing sampling rate of 300 Hz, the amplitude of the “instantaneous” response is  $21.3 + 197 = 218 \text{ nL cm}^{-2} \text{ s}^{-1}$  corresponding to an apparent osmotic permeability,  $P_f^{am} = 4,037 \mu\text{m s}^{-1}$ . This is significantly larger than the estimate

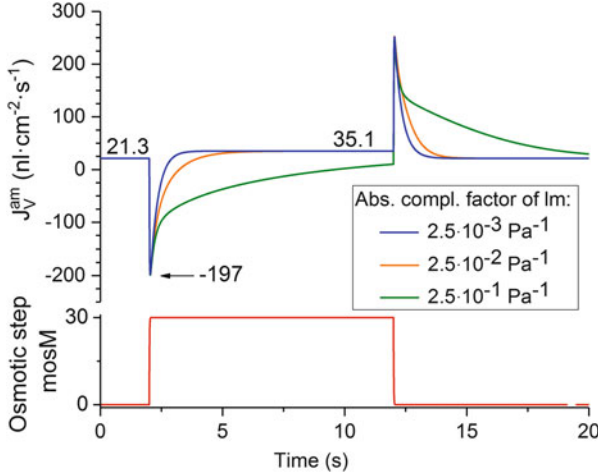


**Fig. 12** Dependence of transient states of intraepithelial water fluxes on compliance factors of lateral intercellular membrane. *Bottom panel* applied luminal 10-s pulse of 30 mosM of non-permeable electroneutral solute. Time constant of rise time,  $\tau = 0.01$  s, sampling rate = 300 Hz. *Upper panel*, compliance factor-dependent relaxation of water flux redistribution between cells and *lis* with  $Vol^{lis} = Vol^{lis, ref} [1 + \mu^{lm} (p^{lis} - p^{cell})]$  (Eq. 18). Blue graph is given by standard input variables. Due to the very fast redirection of intraepithelial water fluxes, the peak response at the onset of the pulse of,  $-197$   $\text{nL cm}^{-2} \text{s}^{-1}$ , is underestimating the apical membrane's water permeability. Thus, the amplitude of the “instantaneous” response is  $-197 - 21.3 = \sim 218$   $\text{nL cm}^{-2} \text{s}^{-1}$  corresponding to an apparent osmotic permeability of apical membrane,  $P_f^{am} = 4,037$   $\mu\text{m s}^{-1}$ , as compared to the true  $P_f^{am} = 4,490$   $\mu\text{m s}^{-1}$

provided by the method of Fig. 11, and much closer to, but not identical with the model's permeability of,  $P_f^{am} = 4,490$   $\mu\text{m s}^{-1}$ . This is not due to the sampling rate of 300 Hz being too slow (not shown), but because the osmotic permeability of the “network” of epithelial membranes distributes “instantaneously” water fluxes between intraepithelial compartments. This is illustrated in Fig. 13a–d, where the analysis is extended for covering all intraepithelial water fluxes. Quasi-stationary states are achieved for all fluxes within the pulse length of 10 s; the numbers given in the four panels verify consistency of intraepithelial fluxes.

### 3.8 Isosmotic Transport

The present study shows that a physiological variation of the rate of fluid absorption by proximal tubule of constant osmotic membrane permeabilities results in predictable variation in osmolarity of transported fluid. For example, an osmolarity of transported fluid of 316 mosM becomes 335 mosM when the rate of fluid absorption is increased by adding glucose to the external solutions (Figs. 2 and 4). Decreasing the osmotic permeability of the luminal membrane also increased the hyperosmolarity, e.g., from 316 to 359 mosM (Figs. 6 and 7). In vitro, the proximal



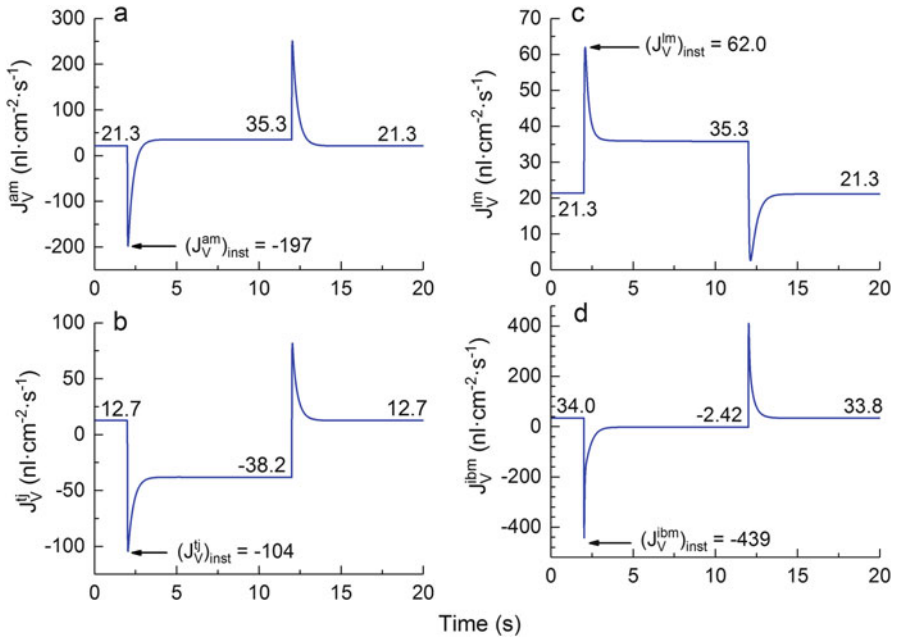


**Fig. 13 (a–d)** Response of intraepithelial water fluxes to luminally applied 30-mosM pulse. The pulse applied is defined in Fig. 10a. **(a)** Water flux across apical membrane; graph is that of Fig. 10 with  $\mu^{lm} = 2.5 \times 10^{-3} \text{ Pa}^{-1}$ . **(b)** Water flux in tight junction is directed toward hyperosmotic luminal bath. In quasi-stationary state,  $J_V^{ij} = -38.2 \text{ nL cm}^{-2} \text{ s}^{-1}$ , illustrating that it is energized by the hyperosmotic pulse. **(c)** Water flux across plasma membrane lining the lateral intercellular space is positive from cell to *lis*.  $J_V^{lm}$  added to the tight junction flux ( $J_V^{ij}$ ) leaves the epithelium across *ibm* to the serosal bath. **(d)** Water flux across the intercellular basement membrane into serosal compartment. The small difference in water fluxes at  $t = 0 \text{ s}$  and  $t = 20 \text{ s}$ , respectively, reflects that intraepithelial ion and volume redistributions are too slow for bringing the epithelium back to its initial steady state (details not shown)

tubule accomplishes isosmotic transport independent of the presence of glucose in luminal perfusion solution. Thus, the above computations show that our model cannot provide an isosmotic absorbate for a given set of osmotic permeabilities. This is an important finding because it indicates that isosmotic absorption is achieved by regulation at epithelial cell level. In an experimental study designed by Ussing of the mechanism of isosmotic transport by the small intestine, Nedergaard et al. (1999) observed that sodium ions are recirculated from the serosal solution via cells back into the lateral intercellular space, which suggested a mechanism for regulating the osmolarity of the transported fluid. In the small intestine (Larsen et al. 2002) and amphibian skin (Larsen et al. 2009), the recirculation pathway would be the 1Na:2Cl:1K cotransporter studied by Frizzell et al. (1979), Ferreira and Ferreira (1981), and Ussing (1985), respectively. In the heterocellular proximal tubule with absorption of  $\text{Na}^+$ ,  $\text{Cl}^-$ , and  $\text{HCO}_3^-$ , one would expect that different segments handle recirculation by different cotransporters depending on whether  $\text{Cl}^-$  or  $\text{HCO}_3^-$  are transported together with  $\text{Na}^+$ . For illustrating the

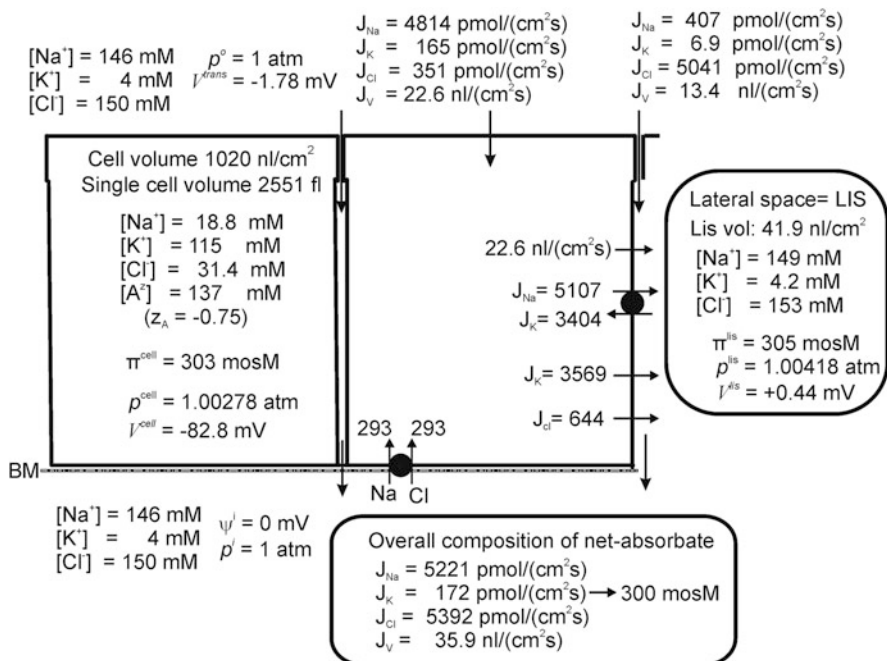


**Fig. 14** The  $Na^+$  recirculation theory applied to the kidney proximal tubule. Model solution illustrating how truly isosmotic transport is achieved by recirculating  $Na^+$  and  $Cl^-$  from the serosal compartment back into the lateral intercellular coupling compartment energized by lateral  $3Na^+/2K^+$ -pumps. Independent variables of all membrane pathways are similar to those used in computations of Fig. 2 in which the serosal  $1Na:1Cl$  cotransporter is quiescent. Turning on regulated  $1Na:1Cl$  cotransport corrected the hyperosmotic absorbate emerging from the lateral space to an overall osmolarity of the absorbate of 300 mosM. It should be noted that the  $1Na:1Cl$  cotransporter is considered here just for the purpose of illustration

significance of regulated ion recirculation in the minimalistic model of the proximal tubule, we introduced a  $1Na:1Cl$  cotransporter of the serosal membrane and adjusted the fluxes carried by this transporter until an overall isosmotic fluid transport was achieved. The result is shown in Fig. 14. It can be seen that a recirculation of  $J_{NaCl}^{sm} = -293 \text{ pmol cm}^{-2} \text{ s}^{-1}$  results in truly isosmotic transport of 300 mosM; this is associated with an increase of  $C_{Na}^{cell}$  from 16.2 to 18.8 mM and an increase of  $C_{Cl}^{cell}$  from 21.8 to 31.4 mM. The concomitant increase in active  $Na^+$  pump flux from 4,816 to 5,107  $\text{pmol cm}^{-2} \text{ s}^{-1}$  indicates that the extra metabolic load of generating truly isosmotic transport would be modest,  $100 (5,107 - 4,816)/4,816 = 6.0\%$ , compared to the results of Fig. 2 obtained with no recirculation.

## 4 Discussion

Our previously published analytical model of transporting epithelia (Larsen et al. 2002) is here extended for analyzing transient states evoked by perturbing independent variables for simulating commonly applied experimental protocols. This has allowed us to deal with time-dependent dynamic interactions of ion and water fluxes through the epithelium and, for the first time, between subepithelial compartments. The updated model also contains equations for the  $\text{Na}^+/\text{K}^+$  pump and the  $\text{Na}^+$ -glucose transporter (SGLT2) with new equations for these transport systems' contribution to the electrical conductance of the plasma membranes. The model was shown to be quite sufficient for giving answers to a number of pertinent problems in kidney physiology that presupposes quantitative biophysical analysis. The check on these points was provided by comparing published experimental observations with predictions given by the model.

### 4.1 *The Coupling Between Active Sodium Transport and Fluid Uptake*

The model reproduces a large number of observations based on a physiologically plausible set of input variables such as intracellular ion composition, membrane potentials and resistances, cell volumes, and transepithelial fluxes of water and ions all in agreement with proximal convoluted tubule in situ and microperfused tubule segments (Figs. 2 and 4). Ion composition, hydrostatic pressure, and volume of the lateral intercellular space, inaccessible to measurements in a transporting epithelium, are obtained at any physiological condition. The convection-electrodiffusion equation for tight junction transport provides basis for discussion of leak fluxes associated the reabsorption of the major fraction of the ultrafiltrate. Interestingly, based upon the convection-electrodiffusion equation (Eq. 6), calculations shown in Figs. 4 and 6 and in Table 1 predict as a novel result that passive back leaks would be prevented by solvent drag in tight junctions in the initial segment of proximal tubule, where the electrochemical driving force otherwise would return a component of the  $\text{Na}^+$  flux to the tubule lumen.

This seems to be a suitable point at which to emphasize that absorption by proximal tubule of  $\text{K}^+$  requires active uptake mechanism, here given by Eq. (2a), because paracellular solvent drag turned out to be quite insufficient, see Sect. 3.1, underscoring the importance of the experimental study by Wilson et al. (1997). By choosing appropriate value of the intrinsic parameter,  $K^{\text{NaK2Cl}, am}$  of Eq. (2a) we could direct the overall transepithelial  $\text{K}^+$  absorption so that the potassium ion concentration of the absorbate becoming close to that of the interstitial fluid. [Results of such a use of the model are independent of the molecular mechanism of active  $\text{K}^+$  uptake]. Thus, governed by the same value of  $K^{\text{NaK2Cl}, am}$  in Figs. 2 and 4, the  $\text{K}^+$  concentration of the absorbate calculates to be 5.2 and 4.1 mM, respectively. With a

fluid absorption rate of 120 l/day by proximal tubule of human kidney the extracellular  $K^+$  concentration could possibly not be maintained within physiological values unless the  $[K^+]$  of the absorbate is regulated at epithelial cell level to be within a range not much different from the physiological range stated to be between 3.8 and 5.0 mM (Hall 2016). By emphasizing the necessity of active  $K^+$  absorption by proximal tubule and the significance of achieving a  $[K^+]$  of the absorbate that is not much different from that of the serosal fluid our analysis has pointed out two important questions for future studies: (1) identification of the molecular mechanism of active transport across the apical membrane, and (2) disclosure of the nature of coordination of the *rate* of fluid absorption and the *flux* of  $K^+$  absorption, respectively, for securing near-extracellular  $[K^+]$  of the absorbate.

The model predicts the well-established stimulation of  $Na^+$ - and fluid absorption by glucose (Figs. 4 and 5). Of particular interest, the new kinetics- and conductance-equations for SGLT2 (Eqs. 3a, 3c) predict the membrane depolarization and decrease in apical membrane resistance caused by glucose absorption, as observed in a microelectrode study by Frömter (1982). With reference to Fig. 4, computed for 5 mM external glucose, the reversal potential of the SGLT2 transporter is given by the expression (cf. Methods),

$$\begin{aligned} E_{rev}^{Glu-Na, am} &= \frac{RT}{F} \ln \frac{C_{Glu}^o \cdot C_{Na^+}^o}{C_{Glu}^{cell} \cdot C_{Na^+}^{cell}} \\ &= 10^3 \times \frac{8.31 \cdot 310}{96485} \ln \frac{5 \cdot 146}{11.8 \cdot 28.2} \\ &= 21.0 \text{ mV} \end{aligned}$$

This is 100 mV above the membrane potential of  $-79$  mV indicating that our conclusion of glucose absorption by the reversible SGLT2 is robust. It is a new and physiologically significant finding of our study that the voltage dependence of the active  $Na^+$  flux (Eq. 4a) predicts an overlooked “cross-talk” mechanism between apical rheogenic  $Na^+$  uptake and active  $Na^+/K^+$  pump fluxes across the lateral membrane. The physiological implication of this mechanism is indicated by the secondary effect on rate of fluid uptake and a higher osmolarity of the fluid exiting the epithelium via the lateral intercellular space (Fig. 4).

## 4.2 Eliminating the Osmotic Permeability of Apical Membrane

An intriguing result was obtained when a simulation of aquaporin knock-out showed that water uptake at transepithelial osmotic equilibrium is not significantly changed after elimination of the osmotic permeability of the apical membrane:  $J_V = 34.0 \text{ nL cm}^{-2} \text{ s}^{-1}$  for  $P_f^{am} = 4,490 \text{ } \mu\text{m s}^{-1}$  and  $J_V = 35.4 \text{ nL cm}^{-2} \text{ s}^{-1}$  for

$P_f^{am} = 0.449 \mu\text{m s}^{-1}$ , respectively (Figs. 2 and 6). This maneuver effectively blocked the translateral water flux and forced the water absorption to be entirely paracellular (Fig. 6). This response was analyzed in detail by following the development of nonstationary states toward the new steady state. By predicting an increase in the osmolarity of the lateral intercellular space, the analysis provided the biophysical mechanism for the large increase in osmolarity of the absorbate (Fig. 7). The experimental study by Schnermann et al. (1998) showed that AQP-1-null mice exhibited a tubular fluid absorption that is 50% of that of AQP-1(+/-) mice. In our analysis of this finding, we showed that the rate of fluid absorption is given by the rate at which sodium ions are pumped into the lateral intercellular space, independent of the pathway taken by water (Figs. 8 and 9). Therefore, we can conclude that the observed significant decrease in rate of fluid absorption in AQP-1(-/-) mice has to be ascribed solely to the authors' concomitantly reported reduction in active  $\text{Na}^+$  absorption. The computed relationship between transepithelial water uptake and active flux of sodium ions (Fig. 9) is a general and fundamental feature of fluid transporting epithelia.

The general applicability of the present study is underscored by pointing out that our analysis eliminates the paradox discussed by Wittekindt and Dietl (2019) that aquaporins in the lung facilitate osmotic water transport, whereas their contribution to water fluxes at near-isosmotic conditions was concluded "elusive." Our analysis of this problem leads to the conclusion that also in the lung are aquaporins of physiological importance for isosmotic transport with the rate of water transport given by the active sodium flux, that is, not by expression of aquaporins. This applies to AQP-1(-/-) engineered lung epithelia as well where the water flow is redirected to the paracellular pathway at a rate given by the active  $\text{Na}^+$  flux (conf. Figs. 2 and 6).

### ***4.3 Transepithelial Osmotic Permeability Versus Osmotic Permeability of Individual Membranes***

The substantial discrepancy between the osmotic permeability of the epithelium obtained by transepithelial osmotic step experiments and the significantly larger experimentally estimated osmotic permeabilities of individual plasma membranes (Carpi-Medina et al. 1984; Gonz ales et al. 1984; Schafer et al. 1978) was characterized by Weinstein (2013) as "one of the confusing features" of epithelia specialized for isosmotic transport. Our analysis provided the mechanistic explanation for this "confusing feature" by revealing how lateral  $\text{Na}^+/\text{K}^+$  pumps on a time scale of about 1 s energize redistribution of water flows between intraepithelial compartments that in the end results in relatively small changes in transepithelial water fluxes and uphill water transport across the epithelium (Figs. 11, 12 and 13). This result illustrates the advantage of our dynamic model over and above the steady-state model of Weinstein (2013) which requires a hypotonic luminal space for generating an absorbed fluid that is "isosmotic to plasma." Our computational analytical method providing time-dependent states of physical variables enabled us to study the time course of

intraepithelial water redistributions that result from an imposed external osmotic pulse. Obviously, a “transepithelial osmotic permeability” calculated from this type of experimental protocol is inadequate for functional characterization of the transporting epithelium (Figs. 9 and 12). Furthermore, the result of our analysis shows that Weinstein’s concept of “intraepithelial solute polarization” cannot be ascribed physical significance. In conclusion, it is a result of significant physiological implications that the osmotic permeability of the whole epithelium  $P_f^{epi}$  has ambiguous biophysical meaning and should be abandoned in studies of water fluxes across intact epithelia.

#### 4.4 *Truly Isosmotic Transport*

In the standing gradient theory of isosmotic transport by Diamond and Bossert (1967), sodium pumps are located in the closed apical end of the lateral intercellular space. It was hypothesized that for a particular set of independent variables such as active pumping rate, diffusion coefficients in *lis* of unstirred fluid, and physical dimensions of the space, this model would have capacity to generate isosmotic transport. The theory directed fresh approaches to the problem of solute-coupled fluid transport and broadened the field by including epithelia of a larger number of animal species adapted to a variety of habitats as reviewed in Berridge and Oschmann (1972). The theory is now abandoned because pumps are uniformly distributed in the lateral membrane or concentrated near the basal end, tight junctions are permeable to both ions and water, and the lateral space cannot be assumed unstirred. Importantly, however, Diamond and Bossert’s theoretical approach gave rise to a clear formulation of the fundamental problem of isosmotic transport. In the authors’ own words (*loc. cit.* page 2077), “two forces are responsible for carrying solute out the open mouth of the system: the diffusion of solute down its concentration gradient, and the sweeping effect of water flow upon solute. Any factor that increases the relative importance of diffusion will make the emergent fluid more hypertonic, while factors increasing the relative importance of water flow are associated with a more nearly isotonic emergent fluid.”

Mathematical models of today are significantly different from the Diamond and Bossert model; the fluid of the lateral intercellular space is assumed well stirred, tight junctions are ion- and water permeable, a basement membrane is separating *lis* and serosal compartment, and hydrostatic pressures and membrane potentials constitute driving forces for water and ion flows. Furthermore, in our treatment of convection-electrodifffusion at the interfaces limiting the lateral intercellular space from outside and inside compartments, respectively, we introduced an expanded version of Hertz’ equation (Larsen et al. 2002). Nevertheless, in general terms, our computations underscored the above conclusion of the Diamond-Bossert paper.

A study applying the pre-steady-state theorem (Sten-Knudsen and Ussing 1981) for separating paracellular and transcellular radioactive  $\text{Na}^+$  fluxes in small intestine

indicated recirculation of sodium ions from serosal solution bath back into lateral space via the transporting epithelial cells (Nedergaard et al. 1999). Our subsequent theoretical analysis (Larsen et al. 2002) indicated that the fairly large recirculation fluxes of the above study follow logically from the relatively small osmotic permeability of small intestine. The present study indicates that in the highly water permeable proximal tubule the putative  $\text{Na}^+$  recirculation flux necessary for isotonic transport would be small and probably too small for being measured. This prediction focuses future research on the precise nature and operation of the serosal  $\text{Na}^+$  cotransporters that may mediate  $\text{Na}^+$  recirculation in the different segments of proximal tubule.

## 5 Additional Information

### Competing Interests

None declared.

### Author Contributions

EHL contributed to the conception of the work. JNS developed the FORTRAN program including the numerical methods. EHL provided mathematical equations, performed most of the computations, and wrote the first draft of the manuscript that was further edited by both authors. Both authors have approved the final version of the manuscript and agree to be accountable for all aspects of the work and qualify for authorship. No one else qualify for authorship.

### Funding

This work was supported by grant CF17-0186 from the Carlsberg Foundation.

## Appendix 1: Nomenclature

See also overview in Fig. 1b.

Variables or constants and their definition	Symbol
Concentration of $j$ ( $\text{Na}^+$ , $\text{K}^+$ , $\text{Cl}^-$ , $\text{A}^-$ , or <i>glucose</i> ) in compartment $comp$ ( $o$ , $cell$ , $lis$ , or $i$ )	$C_j^{comp}$
Osmolarity of compartment indicated by superscript ( $o$ , $cell$ , $lis$ , or $i$ )	$\pi^{comp}$
Hydrostatic pressure of compartment indicated ( $o$ , $cell$ , $lis$ , or $i$ )	$p^{comp}$
Electrical potential of compartment indicated ( $o$ , $cell$ , $lis$ , or $i$ ) with $\psi^i \equiv 0$	$\psi^{comp}$
Transepithelial potential difference, $\psi^o - \psi^i$	$V^{trans}$
Electrical potential difference between $o$ and $cell$ , $\psi^o - \psi^{cell}$	$V^{om}$
Electrical potential difference between $cell$ and $lis$ , $\psi^{cell} - \psi^{lis}$	$V^{lm}$
Electrical potential difference between $cell$ and $i$ , $\psi^{cell} - \psi^i$	$V^{sm}$

(continued)

Variables or constants and their definition	Symbol
Passive permeability of $j$ in membrane $m$ ( $am, lm, sm, tj, ibm$ )	$P_j^m$
Reflection coefficient of $j$ ( $\text{Na}^+, \text{K}^+, \text{Cl}^-, \text{glucose}$ ) in $m$ ( $tj, ibm$ )	$\sigma_j^m$
Flux of $j$ ( $= \text{Na}^+, \text{K}^+, \text{Cl}^-, \text{glucose}$ ) across $m$ ( $am, lm, sm, tj, ibm$ )	$J_j^m$
Electrical current carried by $j$ ( $\text{Na}^+, \text{K}^+, \text{Cl}^-$ ) across $m$ ( $am, lm, sm, tj, ibm$ )	$I_j^m$
Integral ion ( $j$ ) conductance of membrane $m$	$G_j^m$
Water volume flux across $m$ ( $am, lm, sm, tj, ibm$ )	$J_V^m$
Hydraulic conductance of membrane $m$ ( $am, lm, sm, tj, ibm$ )	$L^m$
Osmotic permeability of $m$ ( $am, lm, sm, tj, ibm$ )	$P_f^m$
Relative compliance constant of membrane $m$ ( $am, lm, sm$ )	$\mu^m$
Absolute compliance constant of $lm$	$\bar{\mu}^{lm}$
Empirical constant of 1Na:1K:2Cl cotransporter of membrane $m$	$K_{\text{NaK2Cl}, m}^{\text{Na}}$
Empirical constant of 1Na:1Cl cotransporter of membrane $m$	$K_{\text{NaCl}, m}^{\text{Na}}$
Apparent dissociation constants of $\text{Na}^+$ binding of $\text{Na}^+/\text{K}^+$ pump at $lm$	$K_{\text{Na}^+}^{\text{pump}, lm}$
Apparent dissociation constants of $\text{K}^+$ binding of $\text{Na}^+/\text{K}^+$ pump at $lm$	$K_{\text{K}^+}^{\text{pump}, lm}$
Turnover constant of $\text{Na}^+:\text{glucose}$ transporter at $am$	$P_{\text{Glu-Na}^+}$
Empirical apparent dissociation constant of $\text{Na}^+:\text{glucose}$ transporter at $am$	$K_{\text{Glu-Na}^+}^{\text{Glu-Na}}$
Empirical apparent dissociation constant for glucose of $\text{Na}^+:\text{glucose}$ transporter at $am$	$K_{\text{Na}^+}^{\text{Glu-Na}}$
Maximum turnover of glucose exchanger at $lm$	$J_{\text{Glu}}^{\text{max}, lm}$
App dissociation const. of symmetrical carrier at $lm$	$K_{\text{Glu}}^{lm}$
Turnover constant of $\text{Na}^+:\text{glucose}$ transporter at $am$	$P_{\text{Glu-Na}^+}$
Temperature in K	$T$
Faraday	$F$
Universal gas constant	$R$

## Appendix 2: Independent Variables

Name	Symbol	Value	MKSA unit
Hydraulic conductance of $am$	$L^{am}$	3.1370d-11	$\text{m}^3 \text{s}^{-1} \text{N}^{-1}$
Hydraulic conductance of $sm$	$L^{sm}$	3.5000d-14	$\text{m}^3 \text{s}^{-1} \text{N}^{-1}$
Hydraulic conductance of $lm$	$L^{lm}$	3.4980d-11	$\text{m}^3 \text{s}^{-1} \text{N}^{-1}$
Hydraulic conductance of $tj$	$L^{tj}$	3.1370d-11	$\text{m}^3 \text{s}^{-1} \text{N}^{-1}$
Hydraulic conductance of $ibm$	$L^{ibm}$	2.3100d-07	$\text{m}^3 \text{s}^{-1} \text{N}^{-1}$
$\text{Na}^+$ concentration of outside compartment	$C_{\text{Na}}^o$	146	$\text{mol m}^{-3}$
$\text{K}^+$ concentration of outside compartment	$C_{\text{K}}^o$	4	$\text{mol m}^{-3}$
$\text{Cl}^-$ concentration of outside compartment	$C_{\text{Cl}}^o$	150	$\text{mol m}^{-3}$
Concentration of non-diffusible solute of outside compartment	$C_S^o$	Protocol dependent	$\text{mol m}^{-3}$
Glucose concentration of outside compartment	$C_{\text{glu}}^o$	0, 3 or 5	$\text{mol m}^{-3}$

(continued)



Name	Symbol	Value	MKSA unit
Na <sup>+</sup> concentration of inside compartment	$C_{Na}^i$	146	mol m <sup>-3</sup>
K <sup>+</sup> concentration of inside compartment	$C_K^i$	4	mol m <sup>-3</sup>
Cl <sup>-</sup> concentration of inside compartment	$C_{Cl}^i$	150	mol m <sup>-3</sup>
Concentration of non-diffusible solute of inside comp.	$C_S^i$	0	mol m <sup>-3</sup>
Glucose concentration of inside compartment	$C_{glu}^i$	0, 3, or 5	mol m <sup>-3</sup>
Na <sup>+</sup> GHK permeability of <i>am</i>	$P_{Na}^{am}$	0.100d-6	m s <sup>-1</sup>
K <sup>+</sup> GHK permeability of <i>am</i>	$P_K^{am}$	0.274d-12	m s <sup>-1</sup>
Cl <sup>-</sup> GHK permeability of <i>am</i>	$P_{Cl}^{am}$	0.160d-11	m s <sup>-1</sup>
Na <sup>+</sup> GHK permeability of <i>sm</i>	$P_{Na}^{sm}$	0.100d-11	m s <sup>-1</sup>
K <sup>+</sup> GHK permeability of <i>sm</i>	$P_K^{sm}$	0.100d-11	m s <sup>-1</sup>
Cl <sup>-</sup> GHK permeability of <i>sm</i>	$P_{Cl}^{sm}$	0.100d-11	m s <sup>-1</sup>
Na <sup>+</sup> GHK permeability of <i>lm</i>	$P_{Na}^{lm}$	0.300d-12	m s <sup>-1</sup>
K <sup>+</sup> GHK permeability of <i>lm</i>	$P_K^{lm}$	0.120d-6	m s <sup>-1</sup>
Cl <sup>-</sup> GHK permeability of <i>lm</i>	$P_{Cl}^{lm}$	0.800d-7	m s <sup>-1</sup>
Na <sup>+</sup> GHK permeability of <i>tj</i>	$P_{Na}^{tj}$	0.125d-6	m s <sup>-1</sup>
K <sup>+</sup> GHK permeability of <i>tj</i>	$P_K^{tj}$	0.180d-6	m s <sup>-1</sup>
Cl <sup>-</sup> GHK permeability of <i>tj</i>	$P_{Cl}^{tj}$	0.400d-5	m s <sup>-1</sup>
Glucose permeability of <i>tj</i>	$P_{glu}^{ibm}$	0.950d-8	m s <sup>-1</sup>
Na <sup>+</sup> GHK permeability of <i>ibm</i>	$P_{Na}^{ibm}$	0.750d-6	m s <sup>-1</sup>
K <sup>+</sup> GHK permeability of <i>ibm</i>	$P_K^{ibm}$	0.110d-5	m s <sup>-1</sup>
Cl <sup>-</sup> GHK permeability of <i>ibm</i>	$P_{Cl}^{ibm}$	0.159d-4	m s <sup>-1</sup>
Glucose permeability if <i>ibm</i>	$P_{glu}^{ibm}$	0.350d-5	m s <sup>-1</sup>
1Na:1 K:2Cl co-transporter constant of <i>am</i>	$K^{NaK2Cl, am}$	0.150d-12	m <sup>10</sup> s <sup>-1</sup> mol <sup>-3</sup>
1Na:1Cl co-transporter constant of <i>am</i>	$K^{NaCl, am}$	0.100d-10	m <sup>4</sup> s <sup>-1</sup> mol <sup>-1</sup>
Turnover constant of lateral 3Na <sup>+</sup> /2K <sup>+</sup> pump	$P_{Na^+, K^+}^{pump, lm}$	0.100d-2	mol s <sup>-1</sup> m <sup>-2</sup>
Electromotive force of the 3Na <sup>+</sup> /2K <sup>+</sup> pump	$E^{pump}$	0.2	Volt
Apparent dissociation constants of Na <sup>+</sup> binding	$K_{Na^+}^{pump, lm}$	3.40d0	mol m <sup>-3</sup>
Apparent dissociation constants of K <sup>+</sup> binding	$K_{K^+}^{pump, lm}$	0.75d0	mol m <sup>-3</sup>
Turnover constant of Na <sup>+</sup> :glucose transporter of <i>am</i>	$P^{Glu-Na^+}$	1.6d-8	mol s <sup>-1</sup> m <sup>-2</sup>
Apparent dissociation constant for Na <sup>+</sup>	$K_{Glu}^{Glu-Na}$	5.d0	mol m <sup>-3</sup>
Apparent dissociation constant for glucose	$K_{Na^+}^{Glu-Na}$	0.25d2	mol m <sup>-3</sup>
Maximum turnover of glucose exchanger at <i>lm</i>	$J_{Glu}^{max, lm}$	2.0d-4	mol s <sup>-1</sup> m <sup>-2</sup>
App dissociation const. of symmetry. carrier at <i>lm</i>	$K_{Glu}^{lm}$	5.0d1	mol m <sup>-3</sup>
Hydrostatic pressure of outside compartment	$p^o$	1.01325e5	Pa

(continued)

Name	Symbol	Value	MKSA unit
Hydrostatic pressure of inside compartment	$p^i$	1.01325e5	Pa
Electrical potential of inside compartment	$\psi^i$	0	Volt
Mean valence of nondiffusible intracellular anions	$z_A$	-0.75	
Na <sup>+</sup> reflection coefficient of <i>tj</i>	$\sigma_{Na}^{tj}$	0.70	
K <sup>+</sup> reflection coefficient of <i>tj</i>	$\sigma_K^{tj}$	0.70	
Cl <sup>-</sup> reflection coefficient of <i>tj</i>	$\sigma_{Cl}^{tj}$	0.45	
Glucose reflection coefficient of <i>tj</i>	$\sigma_{Glu}^{tj}$	0.80	
Na <sup>+</sup> reflection coefficient of <i>ibm</i>	$\sigma_{Na}^{ibm}$	0.03	
K <sup>+</sup> reflection coefficient of <i>ibm</i>	$\sigma_K^{ibm}$	0.03	
Cl <sup>-</sup> reflection coefficient of <i>ibm</i>	$\sigma_{Cl}^{ibm}$	0.03	
Glucose reflection coefficient of <i>ibm</i>	$\sigma_{Glu}^{ibm}$	0.03	
Temperature	T	310	K
Faraday	$F$	96,485	C mol <sup>-1</sup>
Absolute compliance constant of <i>lm</i>	$\mu^{lm}$	0.250d-2	Pa <sup>-1</sup>
Reference volume of <i>lis</i>	$Vol^{lis,ref}$	3.10d-7	m <sup>3</sup> m <sup>-2</sup>
Cell density	$D^{cell}$	4.00d+9	# cells m <sup>-2</sup>
Nondiffusible anions in cell	$M_A$	3.50d-13	mol cell <sup>-1</sup>

*o* outside (luminal) compartment, *i* inside (serosal) compartment, *am* apical membrane, *lm* lateral membrane, *sm* serosal membrane, *lm* lateral membrane, *tj* tight junctions, *ibm* interspace basement membrane

## References

- Agre P, Christensen EI, Smith BL, Nielsen S (1993a) Distribution of the aquaporin CHIP in secretory and resorptive epithelia and capillary endothelia. *Proc Natl Acad Sci U S A* 90: 7275-7279
- Agre P, Knepper MA, Christensen EI, Smith BL, Nielsen S (1993b) CHIP28 water channels are localized in constitutively water-permeable segments of the nephron. *J Cell Biol* 120:371-383
- Altenberg GA, Reuss L (2013) Mechanisms of water transport across cell membranes and epithelia. In: Alpern RJ, Caplan M, Moe OW (eds) *Seldin and Giebisch's the kidney. Physiology and pathophysiology*. Elsevier/Academic Press, London, pp 95-120
- Amerongen HM, Mack JA, Wilson JM, Neutra MR (1989) Membrane domains of intestinal epithelial-cells - distribution of Na<sup>+</sup>,K<sup>+</sup>-ATPase and the membrane skeleton in adult-rat intestine during fetal development and after epithelial isolation. *J Cell Biol* 109:2129-2138
- Andreoli TE, Schafer JA (1979) External solution driving forces for isotonic fluid absorption in proximal tubules. *Fed Proc* 38:154-160
- Bennett CM, Clapp JR, Berliner RW (1967) Micropuncture study of proximal and distal tubule in dog. *Am J Physiol* 213:1254
- Berridge MJ, Oschmann JL (1972) *Transporting epithelia*. Academic Press, New York/London, pp 1-91
- Borgnia M, Nielsen S, Engel A, Agre P (1999) Cellular and molecular biology of the aquaporin water channels. *Annu Rev Biochem* 68:425-458
- Boron WF, Boulpaep EL (1983a) Intracellular pH regulation in the renal proximal tubule of the salamander. Basolateral HCO<sub>3</sub><sup>-</sup> transport. *J Gen Physiol* 81:53-94

- Boron WF, Boulpaep EL (1983b) Intracellular pH regulation in the renal proximal tubule of the salamander. Na-H exchange. *J Gen Physiol* 81:29–52
- Boron WF, Boulpaep EL (2017) *Medical physiology*, 3rd edn. Elsevier, Philadelphia
- Burg M, Patlak C, Green N, Villey D (1976) Organic solutes in fluid absorption by renal proximal convoluted tubules. *Am J Physiol* 231:627–637
- Carpi-Medina P, Whittombury G (1988) Comparison of transcellular and transepithelial water osmotic permeabilities ( $P_{os}$ ) in the isolated proximal straight tubule (PST) of the rabbit kidney. *Pflugers Arch* 412:66–74
- Carpi-Medina P, Gonzáles E, Whittombury G (1983) Cell osmotic water permeability of isolated rabbit proximal convoluted tubules. *Am J Physiol* 244:F554–F563
- Carpi-Medina P, Lindemann B, Gonzáles E, Whittombury G (1984) The continuous measurement of tubular volume changes in response to step changes in contraluminal osmolarity. *Pflugers Arch* 400:343–348
- Cassola AC, Mollenhauer M, Frömter E (1983) The intracellular chloride activity of rat kidney proximal tubular cells. *Pflugers Arch* 399:259–265
- Curran PF (1960) Na, Cl, and water transport by rat ileum *in vitro*. *J Gen Physiol* 43:1137–1148
- De Weer P, Gadsby DC, Rakowski RF (1988) Voltage dependence of the Na-K pump. *Annu Rev Physiol* 50:225–241
- Diamond JM (1964) Transport of salt and water in rabbit and guinea pig gallbladder. *J Gen Physiol* 48:1–14
- Diamond JM, Bossert WH (1967) Standing-gradient osmotic flow. A mechanism for coupling of water and solute transport in epithelia. *J Gen Physiol* 50:2061–2083
- DiBona DR, Mills JW (1979) Distribution of  $\text{Na}^+$  –pump sites in transporting epithelia. *Fed Proc* 38:134–143
- Dørup J, Maunsbach AB (1997) Three-dimensional organization and segmental ultrastructure of the rat proximal tubules. *Exp Nephrol* 5:305–317
- Edelman A, Curci S, Samarzija I, Fromter E (1978) Determination of intracellular  $\text{K}^+$  activity in rat-kidney proximal tubular cells. *Pflugers Arch* 378(1):37–45
- Eskesen K, Ussing HH (1985) Determination of the electromotive force of active sodium transport in frog skin epithelium (*Rana temporaria*) from presteady-state flux ratio experiments. *J Membr Biol* 86:105–111
- Ferreira KTG, Ferreira HG (1981) The regulation of volume and ion composition in frog skin. *Biochim Biophys Acta* 646:193–202
- Finkelstein A (1987) *Water movement through lipid bilayer, pores, and plasma membranes. Theory and reality*. Wiley, New York/Chisester/Brisbane/Toronto/Singapore, pp 1–228
- Fischbarg J (2010) Fluid transport across leaky epithelia: central role of the tight junction and supporting role of aquaporins. *Physiol Rev* 90:1271–1290
- Frizzell RA, Field M, Schultz SG (1979) Sodium-coupled chloride transport by epithelial tissues. *Am J Physiol* 236:F1–F8
- Fromm M, Piontek J, Rosenthal R, Gunzel D, Krug SM (2017) Tight junctions of the proximal tubule and their channel proteins. *Pflugers Arch* 469:877–887
- Frömter E (1979) The Feldberg lecture 176: solute transport across epithelia: what can we learn from micropuncture studies on kidney tubules? *J Physiol* 288:1–31
- Frömter E (1982) Electrophysiological analysis of rat renal sugar and amino acid transport. I. Basic phenomena. *Pflugers Arch* 393:179–189
- Gadsby DC, Nakao M (1989) Steady-state current-voltage relationship of the Na/K pump in guinea-pig ventricular myocytes. *J Gen Physiol* 94:511–537
- Gaeggeler HP, Guillod Y, Loffing-Cueni D, Loffing J, Rossier BC (2011) Vasopressin-dependent coupling between sodium transport and water flow in a mouse cortical collecting duct cell line. *Kidney Int* 79:843–852
- Garay RP, Garrahan PJ (1973) The interaction of sodium and potassium with the sodium pump in red cells. *J Physiol* 231:297–325
- Garg LC, Knepper MA, Burg MB (1981) Mineralocorticoid effects on Na-K-ATPase in individual nephron segments. *Am J Physiol* 240:F536–F544

- Ghezzi C, Loo DDF, Wright EM (2018) Physiology of renal glucose handling via SGLT1, SGLT2 and GLUT2. *Diabetologia* 61:2087–2097
- Gögelein H, Greger R (1986) Na<sup>+</sup> selective channels in the apical membrane of rabbit late proximal tubules (pars recta). *Pflügers Arch* 406:198–203
- Goldin SM (1977) Active transport of sodium and potassium ions by the sodium and potassium ion-activated adenosine triphosphatase from renal medulla. Reconstitution of the purified enzyme into a well defined in vitro transport system. *J Biol Chem* 252:5630–5642
- Goldman DE (1943) Potential, impedance, and rectification in membranes. *J Gen Physiol* 27:37–60
- González E, Carpi-Medina P, Linares H, Whittombury G (1984) Osmotic water permeability of the apical membrane of proximal straight tubular (PST) cells. *Pflügers Arch* 402:337–339
- Gottschalk CW (1963) Renal tubular function – lessons from micropuncture. *Harvey Lect* 58: 99–124
- Green R, Giebisch G, Unwin R, Weinstein AM (1991) Coupled water transport by rat proximal tubule. *Am J Physiol* 261:F1046–F1054
- Gyory AZ, Kinne R (1971) Energy source for transepithelial sodium transport in rat renal proximal tubules. *Pflügers Arch* 327:234–260
- Hall JE (2016) Guyton and Hall textbook of medical physiology. Philadelphia, PA, Elsevier
- Hertz G (1922) Ein neues Verfahren zur Trennung von Gasgemischen durch Diffusion. *Phys Z* 23:433–434
- Hodgkin AL (1958) The Croonian lecture: ionic movements and electrical activity in giant nerve fibres. *Proc R Soc Lond B Biol Sci* 148:1–37
- Hodgkin AL, Katz B (1949) The effect of sodium ions on the electrical activity of the giant axon of the squid. *J Physiol* 108:37–77
- Hodgkin AL, Keynes RD (1955) Active transport of cations in giant axons from Sepia and Loligo. *J Physiol* 128:28–66
- Hummel CS, Lu C, Loo DD, Hirayama BA, Voss AA, Wright EM (2011) Glucose transport by human renal Na<sup>+</sup>/D-glucose cotransporters SGLT1 and SGLT2. *Am J Physiol* 300:C14–C21
- Jørgensen PL (1980) Sodium and potassium ion pump in kidney tubules. *Physiol Rev* 60:864–917
- Jørgensen PL (1986) Structure, function and regulation of Na,K-ATPase in the kidney. *Kidney Int* 29:10–20
- Karniski LP, Aronson PS (1987) Anion-exchange pathways for Cl<sup>-</sup> transport in rabbit renal microvillus membranes. *Am J Physiol* 253:F513–F521
- Kashgarian M, Biemesderfer D, Caplan M, Forbush B III (1985) Monoclonal antibody to Na, K-ATPase: immunocytochemical localization along nephron segments. *Kidney Int* 28:899–913
- Kirk KL, Schafer JA, DiBona DR (1987) Cell volume regulation in rabbit proximal straight tubule perfused in vitro. *Am J Physiol* 252:F922–F932
- Kokko JP, Burg MB, Orloff J (1971) Characteristics of NaCl and water transport in renal proximal tubule. *J Clin Investig* 50:69
- Lapointe JY, Duplain M (1991) Regulation of basolateral membrane potential after stimulation of Na<sup>+</sup> transport in proximal tubules. *J Membr Biol* 120:165–172
- Larsen EH (1973) Effect of amiloride, cyanide and ouabain on the active transport pathway in toad skin. In: *Transport Mechanisms in Epithelia*, Proc Alfred Benzon Symp, vol V. Munksgaard, Copenhagen, pp 131–147
- Larsen EH (1991) Chloride transport by high-resistance heterocellular epithelia. *Physiol Rev* 71: 235–283
- Larsen EH (2011) Reconciling the Krogh and Ussing interpretations of epithelial chloride transport – presenting a novel hypothesis for the physiological significance of the passive cellular chloride uptake. *Acta Physiol* 202:435–464
- Larsen EH, Sørensen JB, Sørensen JN (2000) A mathematical model of solute coupled water transport in toad intestine incorporating recirculation of the actively transported solute. *J Gen Physiol* 116:101–124
- Larsen EH, Sørensen JB, Sørensen JN (2002) Analysis of the sodium recirculation theory of solute-coupled water transport in small intestine. *J Physiol* 542:33–50
- Larsen EH, Willumsen NJ, Møbjerg N, Sørensen JN (2009) The lateral intercellular space as osmotic coupling compartment in isotonic transport. *Acta Physiol* 195:171–186

- Läuger P (1991) Electrogenic ion pumps. Sinauer Associates, Sunderland, pp 1–313
- Layton AT, Vallon V, Edwards A (2015) Modeling oxygen consumption in the proximal tubule: effects of NHE and SGLT2 inhibition. *Am J Physiol* 308:F1343–F1357
- Low VL, Ferreira HG, Moura T (1979) The behavior of transporting epithelial cells. I. Computer analysis of a basic model. *Proc R Soc Lond B Biol Sci* 206:53–83
- Maunsbach AB (1966) Observations on the segmentation of the proximal tubule in the rat kidney. Comparison of results from phase contrast, fluorescence and electron microscopy. *J Ultrastruct Res* 16:239–258
- Maunsbach AB (1973) Ultrastructure of the proximal tubule. In: Orloff J, Berliner RW (eds) *Handbook of physiology*. American Physiological Society, Washington, DC, pp 31–79
- Maunsbach AB, Boulpaep EL (1991) Immunoelectron microscope localization of Na,K-ATPase in transport pathways in proximal tubule epithelium. *Micron Microsc Acta* 22:55–56
- Mills JW, DiBona DR (1977) On the distribution of Na<sup>+</sup>-pump sites in the frog skin. *J Cell Biol* 75: 968–973
- Mills JW, DiBona DR (1978) Distribution of Na<sup>+</sup>-pump sites in the frog gallbladder. *Nature* 271: 273–275
- Mills JW, Ernst SA, DiBona DR (1977) Localization of Na<sup>+</sup>-pump sites in frog skin. *J Cell Biol* 73: 88–110
- Morel F, Murayama Y (1970) Simultaneous measurement of unidirectional and net sodium fluxes in microperfused rat proximal tubules. *Pflügers Arch* 320:1–23
- Murer H, Hopfer U, Kinne R (1976) Sodium/proton antiport in brush-border-membrane vesicles isolated from rat small intestine and kidney. *Biochem J* 154:597–604
- Nagel W (1980) Rheogenic sodium transport in a tight epithelium, the amphibian skin. *J Physiol* 302:281–295
- Nedergaard S, Larsen EH, Ussing HH (1999) Sodium recirculation and isotonic transport in toad small intestine. *J Membr Biol* 168:241–251
- Nielsen R, Larsen EH (2007) Beta-adrenergic activation of solute coupled water uptake by toad skin epithelium results in near-isosmotic transport. *Comp Biochem Physiol A Mol Integr Physiol* 148A:64–71
- Nielsen S, Kishore BK, Chou C-L, Mandon B, Marples D, Ecelbarger A, Terris J, Wade JB, Knepper MA (1996) Renal aquaporins. *Kidney Int* 49:1712–1717
- Padilla-Benavides T, Roldán ML, Larre I, Flores-Benitez D, Villegas-Sepúlveda N, Contreras RG, Cerejido M, Shoshani L (2010) The polarized distribution of Na<sup>+</sup>,K<sup>+</sup>-ATPase: role of the interaction between β subunits. *Mol Biol Cell* 21(13):2217–2225
- Parent L, Supplisson S, Loo DDF, Wright EM (1992) Electrogenic properties of the cloned Na<sup>+</sup>/glucose cotransporter: I. Voltage-clamp studies. *J Membr Biol* 125:49–62
- Parsons DS, Wingate DL (1958) Fluid movements across the wall of rat small intestine *in vitro*. *Biochim Biophys Acta* 30:666–667
- Reuss L (1985) Changes in cell volume measured with an electrophysiologic technique. *Proc Natl Acad Sci U S A* 82:6014–6018
- Sackin H, Boulpaep EL (1975) Models for coupling of salt and water transport. Proximal tubular reabsorption in necturus kidney. *J Gen Physiol* 66:671–733
- Samarzija I, Hinton BT, Fromter E (1982) Electrophysiological analysis of rat renal sugar and amino acid transport II. Dependence on various transport parameters and inhibitors. *Pflügers Arch* 393(2):190–197
- Sardet C, Franchi A, Pouyssegur J (1989) Molecular cloning, primary structure, and expression of the human growth factor-activatable Na<sup>+</sup>/H<sup>+</sup> antiporter. *Cell* 56:271–280
- Schafer JA (1990) Transepithelial osmolality differences, hydraulic conductivities, and volume absorption in the proximal tubule. *Annu Rev Physiol* 52:709–726
- Schafer JA (1993) The rat collecting duct as an isosmotic volume reabsorber. In: Ussing HH, Fischbarg J, Sten-Knudsen O, Larsen EH, Willumsen NJ (eds) *Proceeding of alfred benzon symposium 34. Isotonic transport in leaky epithelia*. Munksgaard, Copenhagen, pp 339–354
- Schafer JA, Troutman SL, Andreoli TE (1974) Volume reabsorption, transepithelial potential differences, and ionic permeability properties in mammalian superficial proximal straight tubules. *J Gen Physiol* 64:582–607

- Schafer JA, Patlak CS, Troutman SL, Andreoli TE (1978) Volume absorption in the parts recta. II. Hydraulic conductivity coefficient. *Am J Physiol* 234:F340–F348
- Schatzmann HJ, Windhager EE, Solomon AK (1958) Single proximal tubules of the *Necturus* kidney. II. Effect of 2, 4-dinitro-phenol and ouabain on water reabsorption. *Am J Physiol* 195(3):570–574
- Schnermann J, Chou C-L, Ma T, Traynor T, Knepper MA, Verkman AS (1998) Defective proximal tubular fluid reabsorption in transgenic aquaporin-1 null mice. *Proc Natl Acad Sci U S A* 95: 9660–9664
- Schultz SG (1980) The electrochemical potential. In: Hutchinson F, Fuller W, Mullins LJ (eds) *Basic principles of membrane transport*. Cambridge University Press, Cambridge, pp 8–13
- Skou JC (1965) Enzymatic basis for active transport of Na<sup>+</sup> and K<sup>+</sup> across cell membrane. *Physiol Rev* 45:596–617
- Smoluchowski MV (1915) Über Brownsche Molekularbewegung unter Einwirkung äusserer Kräfte und deren Zusammenhang mit der verallgemeinerten Diffusionsgleichung. *Ann Phys* 48:1103–1112
- Spring KR (1999) Epithelial fluid transport – a century of investigation. *News Physiol Sci* 14:92–98
- Spring KR, Hope A (1978) Size and shape of the lateral intercellular spaces in a living epithelium. *Science* 200:54–57
- Spring KR, Kimura G (1978) Chloride reabsorption by renal proximal tubules of *Necturus*. *J Membr Biol* 38:233–254
- Spring KR, Kimura G (1979) Intracellular ion activities in *Necturus* proximal tubule. *Fed Proc* 38:2729–2732
- Stein WD (1967) *The movement of molecules across cell membranes*. Academic Press, New York, pp 1–369
- Sten-Knudsen O (2002) *Biological membranes. Theory of transport, potentials and electric impulses*. Cambridge University Press, Cambridge, pp 1–671
- Sten-Knudsen O, Ussing HH (1981) The flux ratio equation under nonstationary conditions. *J Membr Biol* 63:233–242
- Stirling CE (1972) Radioautographic localization of sodium pump sites in rabbit intestine. *J Cell Biol* 53:704–714
- Thomas RC (1972) Electrogenic sodium pump in nerve and muscle cells. *Physiol Rev* 52:563–594
- Tripathi S, Boulpaep EL (1989) Mechanisms of water transport by epithelial cells. *Q J Exp Physiol* 74:385–417
- Turner RJ, Moran A (1982) Heterogeneity of sodium-dependent D-glucose transport sites along the proximal tubule – evidence from vesicle studies. *Am J Physiol* 242:F406–F414
- Turner RJ, Silverman M (1977) Sugar uptake into brush-border vesicles from normal human kidney. *Proc Natl Acad Sci U S A* 74:2825–2829
- Ullrich KJ (ed) (1973) *Permeability characteristics of the mammalian nephron*. American Physiological Society, Bethesda
- Ussing HH (1985) Volume regulation and basolateral co-transport of sodium, potassium, and chloride ion in frog skin epithelium. *Pflügers Arch* 405(suppl 1):S2–S7
- Warnock DG, Lucci MS (1979) Effect of anion-transport inhibitors on NaCl reabsorption in the rat superficial proximal convoluted tubule. *J Clin Invest* 64:570–579
- Weinstein AM (1985) Glucose-transport in a model of the rat proximal tubule epithelium. *Math Biosci* 76:87–115
- Weinstein AM (1986) A mathematical model of the rat proximal tubule. *Am J Physiol* 250: F860–F873
- Weinstein AM (1992) Chloride transport in a mathematical model of the rat proximal tubule. *Am J Physiol* 263:F784–F798
- Weinstein AM (2013) Sodium and chloride transport: proximal nephron. In: Alpern RJ, Moe OW, Caplan MJ (eds) *Seldin and Giebisch's the kidney*. Elsevier, Amsterdam, pp 1081–1141
- Weinstein AM, Stephenson JL (1979) Electrolyte transport across a simple epithelium. Steady-state and transient analysis. *Biophys J* 27:165–186
- Weinstein AM, Stephenson JL (1981) Models of coupled salt and water transport across leaky epithelia. *J Membr Biol* 60:1–20

- Welling LW, Grantham JJ (1972) Physical properties of isolated perfused renal tubules and tubular basement membranes. *J Clin Invest* 51:1063–1075
- Welling LW, Welling DJ (1975) Surface areas of brush border and lateral cell walls in the rabbit proximal nephron. *Kidney Int* 8:343–348
- Welling LW, Welling DJ (1988) Relationship between structure and function in renal proximal tubule. *J Electron Microscop Tech* 9:171–185
- Welling LW, Welling DJ, Holsapple JW, Evan AP (1987a) Morphometric analysis of distinct microanatomy near the base of proximal tubule cells. *Am J Physiol* 253:F126–F140
- Welling LW, Welling DJ, Ochs TJ (1987b) Video measurement of basolateral NaCl reflection coefficient in proximal tubule. *Am J Physiol* 253:F290–F298
- Whittembury G, Reuss L (1992) Mechanisms of coupling of solute and solvent transport in epithelia. In: Seldin DW, Giebisch G (eds) *Kidney: physiology and pathophysiology*. Raven Press, New York, pp 317–360
- Whittembury G, Malnic G, Mello-Aires M, Amorena C (1988) Solvent drag of sucrose during absorption indicates paracellular water flow in the rat kidney proximal tubule. *Pflugers Arch* 412:541–547
- Wilson RW, Wareing M, Green R (1997) The role of active transport in potassium reabsorption in the proximal convoluted tubule of the anaesthetized rat. *J Physiol* 500:155–164
- Windhager EE (1979) Sodium chloride transport. In: Giebisch G, Tosteson DC, Ussing HH (eds) *Membrane transport in biology, Transport organs, vol IVA*. Springer, Berlin, pp 145–213
- Windhager EE, Whittembury G, Oken DE, Schatzmann HJ, Solomon AK (1959) Single proximal tubules of the Necturus kidney. III. Dependence of H<sub>2</sub>O movement on NaCl concentration. *Am J Physiol* 197:313–318
- Wittekindt OH, Dietl P (2019) Aquaporins in the lung. *Pflugers Arch* 471(4):519–532
- Wu MM, Civan MM (1991) Voltage dependence of current through the Na,K-exchange pump of *Rana* oocytes. *J Membr Biol* 121:23–36
- Yoshitomi K, Fromter E (1985) How big is the electrochemical potential difference of Na<sup>+</sup> across rat renal proximal tubular cell membranes in vivo? *Pflugers Arch* 405(Suppl 1):S121–S126
- Yoshitomi K, Burckhardt BC, Fromter E (1985) Rheogenic sodium-bicarbonate cotransport in the peritubular cell membrane of rat renal proximal tubule. *Pflugers Arch* 405:360–366
- Zeuthen T (2000) Molecular water pumps. *Rev Physiol Biochem Pharmacol* 141:97–151
- Zeuthen T, Meinild AK, Loo DD, Wright EM, Klaerke DA (2001) Isotonic transport by the Na<sup>+</sup>-glucose cotransporter SGLT1 from humans and rabbit. *J Physiol* 531:631–644
- Zhuo JL, Li XC (2013) Proximal nephron. *Compr Physiol* 3:1079–1123
- Zurzolo C, Rodriguezboulan E (1993) Delivery of Na<sup>+</sup>,K<sup>+</sup>-ATPase in polarized epithelial-cells. *Science* 260:550–552

**Open Access** This chapter is licensed under the terms of the Creative Commons Attribution 4.0 International License (<http://creativecommons.org/licenses/by/4.0/>), which permits use, sharing, adaptation, distribution and reproduction in any medium or format, as long as you give appropriate credit to the original author(s) and the source, provide a link to the Creative Commons licence and indicate if changes were made.

The images or other third party material in this chapter are included in the chapter's Creative Commons licence, unless indicated otherwise in a credit line to the material. If material is not included in the chapter's Creative Commons licence and your intended use is not permitted by statutory regulation or exceeds the permitted use, you will need to obtain permission directly from the copyright holder.

